

# Photoconversion and Nuclear Trafficking Cycles Determine Phytochrome A's Response Profile to Far-Red Light

Julia Rausenberger,<sup>1,2,7</sup> Anke Tscheuschler,<sup>2</sup> Wiebke Nordmeier,<sup>5</sup> Florian Wüst,<sup>2</sup> Jens Timmer,<sup>3,4,6</sup> Eberhard Schäfer,<sup>2,4</sup> Christian Fleck,<sup>1,\*</sup> and Andreas Hiltbrunner<sup>5,\*</sup>

<sup>1</sup>Centre for Biological Systems Analysis (ZBSA)

<sup>2</sup>Faculty of Biology

<sup>3</sup>Freiburg Institute for Advanced Studies (FRIAS)

<sup>4</sup>BIOSS Centre for Biological Signalling Studies

University of Freiburg, 79104 Freiburg, Germany

<sup>5</sup>Center for Plant Molecular Biology (ZMBP), University of Tübingen, 72076 Tübingen, Germany

<sup>6</sup>Department of Clinical and Experimental Medicine, Linköping University, SE-581 83 Linköping, Sweden

<sup>7</sup>Present address: School of Life Sciences, University of Applied Sciences Northwestern Switzerland, 4132 Muttenz, Switzerland

\*Correspondence: christian.fleck@fdm.uni-freiburg.de (C.F.), andreas.hiltbrunner@zmbp.uni-tuebingen.de (A.H.)

DOI 10.1016/j.cell.2011.07.023

## SUMMARY

Phytochrome A (phyA) is the only photoreceptor in plants, initiating responses in far-red light and, as such, essential for survival in canopy shade. Although the absorption and the ratio of active versus total phyA are maximal in red light, far-red light is the most efficient trigger of phyA-dependent responses. Using a joint experimental-theoretical approach, we unravel the mechanism underlying this shift of the phyA action peak from red to far-red light and show that it relies on specific molecular interactions rather than on intrinsic changes to phyA's spectral properties. According to our model, the dissociation rate of the phyA-FHY1/FHL nuclear import complex is a principle determinant of the phyA action peak. The findings suggest how higher plants acquired the ability to sense far-red light from an ancestral photoreceptor tuned to respond to red light.

## INTRODUCTION

Light is an abiotic factor, which is particularly important for plants. It is used as a source of energy but also provides information about the environment. To monitor the intensity, quality, and direction of incident light, plants employ different types of photoreceptors, such as the phototropins and cryptochromes, which are blue light (B) receptors, or the red (R)/far-red (FR) light-absorbing phytochromes (Devlin et al., 2007). In *Arabidopsis*, there are five phytochromes (phyA-phyE), among which phyA and phyB are most important. PhyB is the dominating phytochrome species in light-grown and adult plants and plays a role in the shade avoidance response, regulation of flowering, and de-etiolation in R. In contrast, the switch from skotomorpho-

genic (development in the dark) to photomorphogenic (development in light) growth in FR-enriched environments requires phyA, which accumulates to very high levels in etiolated seedlings but is rapidly degraded upon irradiation with light (Bae and Choi, 2008).

Plant phytochromes are dimeric photoreceptors containing a covalently bound open-chain tetrapyrrole as chromophore (Rockwell et al., 2006). They have a photocycle with Pr as the ground state and Pfr as a longer-lived intermediate. Pr is biologically inactive and exhibits maximal absorption in R, whereas Pfr has an absorption peak in FR and is considered the active form of phytochromes. By absorption of light, they can reversibly interconvert between Pr and Pfr via short-lived photochemical intermediates (Mancinelli, 1994; Rockwell et al., 2006). Typically, phyB-mediated responses are induced by R and can be canceled by an FR pulse immediately following the R treatment (Casal et al., 2003). This mode of action, termed low fluence response (LFR), is consistent with a model in which phytochromes work as light switches that can be turned on and off by irradiation with R and FR. However, phyA-mediated responses are induced by very low amounts of light of any wavelength (very low fluence response [VLFR]) or by continuous irradiation with high fluence rate FR (high irradiance response [HIR]) and cannot be explained by a simple light switch (Casal et al., 2003). Although Pr and Pfr have absorption peaks at 667 nm (R) and 730 nm (FR), respectively, they absorb in FR and R as well. Thus, irradiation with either R or FR drives the conversion between Pr and Pfr in both directions. This results in continuous cycling between Pr and Pfr, which establishes the equilibrium between the two conformers depending on the wavelength, but not on the fluence rate (Mancinelli, 1994).

PhyA localizes to the cytosol in the dark and accumulates in the nucleus in response to irradiation with FR (Bae and Choi, 2008). Translocation of phyA into the nucleus is indispensable for FR perception and depends on the two functional homologs FHY1 and FHL, which physically interact with phyA (Hiltbrunner et al., 2005, 2006; Rösler et al., 2007; Shen et al., 2009; Yang

et al., 2009). The amount of phyA accumulating in the nucleus of FR-treated seedlings exceeds the total level of FHY1 and FHL that is available in a cell by several-fold. Therefore, FHY1/FHL have been predicted to work as shuttle proteins that cycle between the cytosol and the nucleus (Genoud et al., 2008).

PhyA is essential for de-etiolation in FR-rich environments, such as in canopy shade, and it may have provided an adaptive advantage to early angiosperms during colonization of habitats dominated by gymnosperms and ferns (Mathews, 2005). Although, as for any other phytochrome, the Pfr/Ptot ratio ( $P_{tot} = P_r + P_{fr}$ ) is much higher in R than in FR, the action spectra for hypocotyl growth inhibition and other high irradiance responses (HIRs) exhibit a peak in the FR range of the spectrum (Figure S1 available online), which is absent in *phyA* mutant plants (Shinomura et al., 2000). Several models have been proposed to explain why maximal photon efficiency is shifted toward FR despite the lower relative abundance of the active Pfr form, but none link the shift to defined components or molecular events (Hennig et al., 1999, 2000; Schäfer, 1975; Shinomura et al., 2000). Interestingly, both HIRs and efficient accumulation of phyA in the nucleus require continuous irradiation with high fluence rate FR; thus, phyA nuclear transport itself can be considered an HIR.

In this work, we show that nucleocytoplasmic shuttling of FHY1/FHL plays a decisive role in phyA signaling and the HIR. Based on this finding, we develop a mathematical model for the HIR that integrates the current knowledge of phyA dynamics, nuclear transport, and interaction with FHY1/FHL. Our investigation shows that the dynamic model of the phyA interaction network intrinsically exhibits the typical features of the HIR and that the principle mechanism underlying the R→FR shift of the peak in the phyA action spectrum can be understood in simple, molecular terms. Finally, the model presented in this report also offers an explanation for the difference in spectral responsiveness of phyA and phyB despite the fact that they have identical photophysical properties.

## RESULTS

### Interaction with phyA Slows Down FHY1 Nucleocytoplasmic Shuttling

FHY1/FHL have been predicted to shuttle between the cytosol and the nucleus in order to transport more than only one phyA per FHY1/FHL (Genoud et al., 2008). We tested this using fluorescence recovery after photobleaching (FRAP) and fluorescence loss in photobleaching (FLIP) assays to analyze the mobility of yellow fluorescent protein (YFP)-tagged FHY1 in etiolated *Arabidopsis* seedlings. These approaches showed that YFP-FHY1 is indeed highly mobile and moves in both directions between the cytosol and the nucleus (Figures 1A and 1B). Interestingly, the mobility of YFP-FHY1 was strongly reduced in seedlings, which had been irradiated for 5 min with R to establish high levels of Pfr, whereas a 5 min R treatment did not affect the YFP-FHY1 mobility in the absence of phyA (Figures 1C and 1D).

### Pfr Is Essential for phyA Nuclear Transport

In FR (730 nm), only about 2% of the total phyA is in Pfr (Mancinelli, 1994). Nevertheless, under these conditions, seedlings

accumulate high levels of phyA in the nucleus, which account for much more than only 2% of the total phyA. This suggests that, in seedlings grown in FR, the major part of phyA in the nucleus is in Pr. However, phyA C323A, which is unable to bind the chromophore and cannot be converted to Pfr (Rockwell et al., 2006) (see Supplemental Information), did not accumulate in the nucleus of *phyA* mutant seedlings, and in yeast two-hybrid assays, it did not interact with FHY1 (Figure 2A and Figure S2). Thus, we conclude that only Pfr can translocate from the cytosol into the nucleus and that all nuclear-localized Pr results from photoconversion of phyA, which has been transported as Pfr.

### Constitutively Active phyA Blocks phyA Nuclear Transport

Recently, Su and Lagarias (2007) described a phyB mutant (Y276H), which is constitutively active. Dark-grown seedlings expressing phyB Y276H exhibited a constitutively photomorphogenic (*cop*) phenotype and resembled de-etiolated wild-type seedlings at the transcriptome level (Hu et al., 2009; Su and Lagarias, 2007). PhyA Y242H-YFP contains a Y-to-H amino acid substitution at position 242, which corresponds to the amino acid change in the phyB Y276H mutant. Expression of phyA Y242H-YFP in wild-type background resulted in a *cop* phenotype as well, which was, however, much less pronounced than in seedlings expressing phyB Y276H (Su and Lagarias, 2007; Figure 3A and Figure S3). qPCR analyses showed that light-induced genes, such as PRR9 or CAB2, are upregulated (PRR9, 3.4-fold; CAB2, 7.0-fold) in dark-grown wild-type seedlings containing phyA Y242H-YFP (Figures 3C and 3D). Interestingly, phyA Y242H-YFP still depends on FHY1/FHL for activity, as *fhv1 fhv1* seedlings expressing phyA Y242H-YFP remained fully etiolated (Figure S3).

In FR, the expression of phyA Y242H-YFP resulted in a strong dominant-negative phenotype (Figures 3A and 3B), which is in agreement with data by Su and Lagarias (2007) but is nevertheless not easy to reconcile with the idea that phyA Y242H-YFP is a constitutively active photoreceptor. Yet, consistent with this finding, phyA Y242H-YFP partially suppressed the upregulation of PRR9 and CAB2 in seedlings exposed to light (Figures 3C and 3D). An important prediction of the FHY1 shuttling model suggested by Genoud et al. (2008) is that any mutation that interferes with FHY1 recycling should interfere with nuclear transport of phyA and, as a consequence, result in reduced sensitivity to FR. The FRAP/FLIP experiments with YFP-FHY1 indicate that high levels of Pfr decrease the mobility of FHY1 (Figure 1). As phyA Y242H-YFP-expressing plants contain high amounts of “Pfr,” nuclear transport of phyA Y242H-YFP may be reduced. Using fluorescence microscopy, we found that only very low levels of phyA Y242H-YFP accumulate in the nucleus, irrespective of whether or not the seedlings were exposed to light (Figure 3E). Moreover, in seedlings coexpressing phyA Y242H-YFP and cyan fluorescent protein (CFP)-tagged wild-type phyA, the “constitutively active” phyA inhibited nuclear transport of phyA-CFP (Figure 3E). As phyA nuclear transport is required for FR signaling (Hiltbrunner et al., 2006; Rösler et al., 2007), these findings can explain the dominant-negative effect of phyA Y242H-YFP in FR.

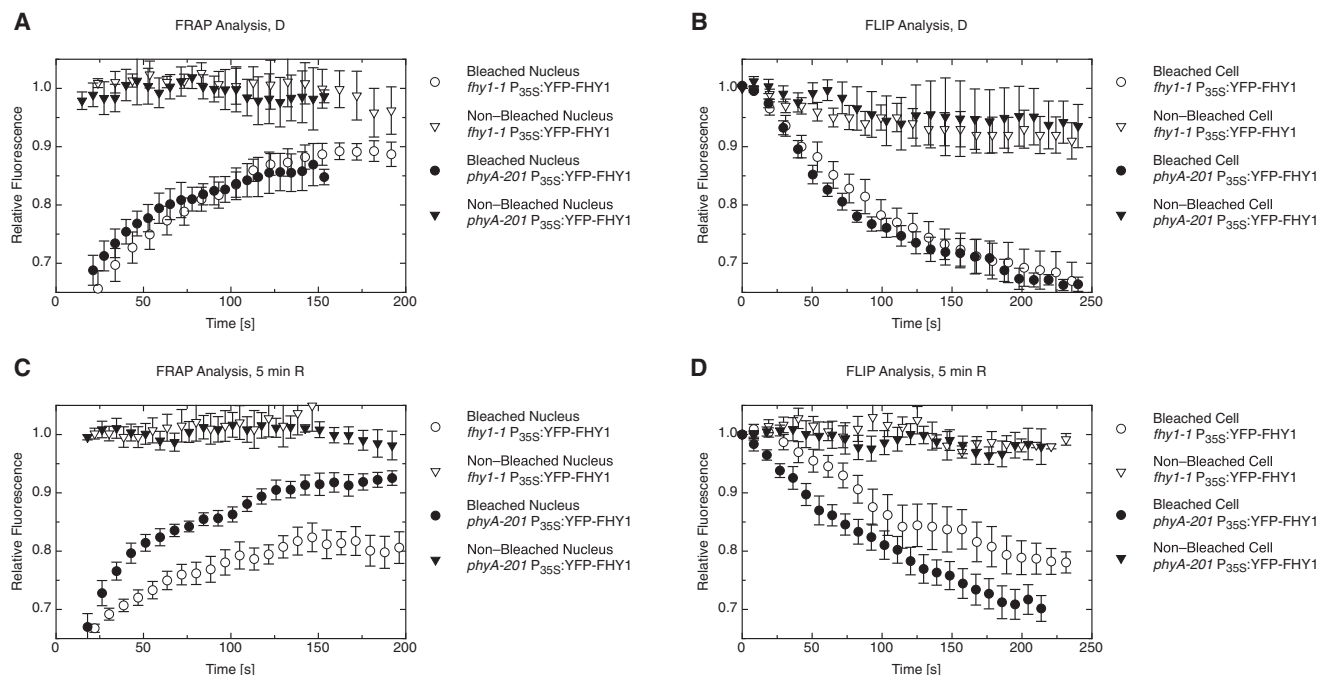


**Figure 1. FHY1 Nucleocytoplasmic Shuttling**

(A and B) FHY1 is mobile between the cytosol and the nucleus.

(A) For FRAP assays, 3-day-old etiolated *fhy1-1* (open symbols) and *phyA-201* seedlings (filled symbols) expressing P<sub>35S</sub>:YFP-FHY1 (YFP-FHY1 under the control of the constitutive 35S promoter) were used. After bleaching the nucleus of a cell, the recovery of the fluorescence was recorded in the bleached nucleus (circles) and, as a control, in a neighboring nonbleached nucleus (triangles). *n* = 6. Error bars represent SEM.

(B) Seedlings for FLIP assays were grown as described in (A). While continuously bleaching an area in the cytosol of a cell, the loss of fluorescence in the nucleus of the same cell was recorded (circles). As a control, the fluorescence in the nucleus of a nonbleached cell was measured (triangles). *n* = 6. Error bars represent SEM.

(C and D) Interaction with *phyA* slows down shuttling of FHY1. (C) Three-day-old etiolated *fhy1-1* (open symbols) and *phyA-201* (filled symbols) seedlings expressing P<sub>35S</sub>:YFP-FHY1 were irradiated for 5 min with R (15  $\mu\text{mol m}^{-2} \text{s}^{-1}$ ) and used for FRAP analyses as described in (A). *n* = 6. Error bars represent SEM.

(D) The seedlings were grown as in (C) and used for FLIP experiments as described in (B). *n* = 6. Error bars represent SEM.

### PhyA Y242H Is Constitutively in the Pfr Form

PhyA Y242H is predicted to be constitutively in Pfr (Su and Lagarias, 2007). In yeast two-hybrid assays, binding of *phyA* to FHY1, FHL, PIF1, and PIF3 was dependent on light, i.e., on conditions establishing high levels of Pfr. In contrast, *phyA* Y242H did interact with FHY1, FHL, PIF1, and PIF3 in a light-independent manner, indicating that it is constitutively in Pfr or at least in a Pfr-like conformation (Figures 2A and 2B). Previously, it was shown that the *phyA*-FHY1/FHL complex rapidly dissociates when *phyA* is converted to Pr (Genoud et al., 2008; Sorokina et al., 2009). In contrast, in yeast two-hybrid assays, *phyA* Y242H-FHY1/FHL complexes were stable irrespective of the light conditions (Figure 2C). This further supports the notion that *phyA* Y242H is constitutively in Pfr and cannot be converted to Pr by any light treatment.

Su and Lagarias (2007) showed that *phyB* Y276H still depends on the chromophore for physiological activity. Consistent with this notion, we found that mutating cysteine 323 in *phyA*, which is essential for chromophore binding, to an alanine (C323A) abolished the interaction of *phyA* Y242H and FHY1 (Figure 2A).

### Mathematical Model Exhibits Maximal Action in FR

Although *phyA* Y242H-YFP is constitutively in Pfr, it is virtually inactive at the physiological level, and seedlings expressing

*phyA* Y242H-YFP exhibit only a weak *cop* phenotype (Figure 3A and Figure S3) (Su and Lagarias, 2007). Thus, not only Pr  $\rightarrow$  Pfr but also Pfr  $\rightarrow$  Pr conversion seems to be essential for proper *phyA* function. Based on these findings, we propose a model for light- and FHY1/FHL-dependent *phyA* nuclear transport, which consists of three overlapping cycles: two Pr/Pfr photoconversion cycles—one in the cytosol and one in the nucleus—and one FHY1/FHL-Pr/Pfr complex association/dissociation cycle, which links the two photoconversion cycles (Figure 4A and Figure S4A). In this model, FHY1/FHL continuously shuttle between the cytosol and the nucleus. They bind reversibly to *phyA* in the cytosol and transport it into the nucleus. After dissociation, FHY1/FHL are recycled back to the cytosol.

Due to the nonlinearity of the system shown in Figure 4A, which arises from the *phyA*-FHY1/FHL complex formation, the dynamics cannot be predicted without a more detailed mathematical analysis. As most of the biochemical parameters of the model depicted in Figure 4A are unknown and difficult to determine experimentally, a qualitative global network analysis was employed (Clodong et al., 2007; von Dassow et al., 2000). The emerging reaction scheme is described by a system of coupled ordinary differential equations (see Supplemental Information).

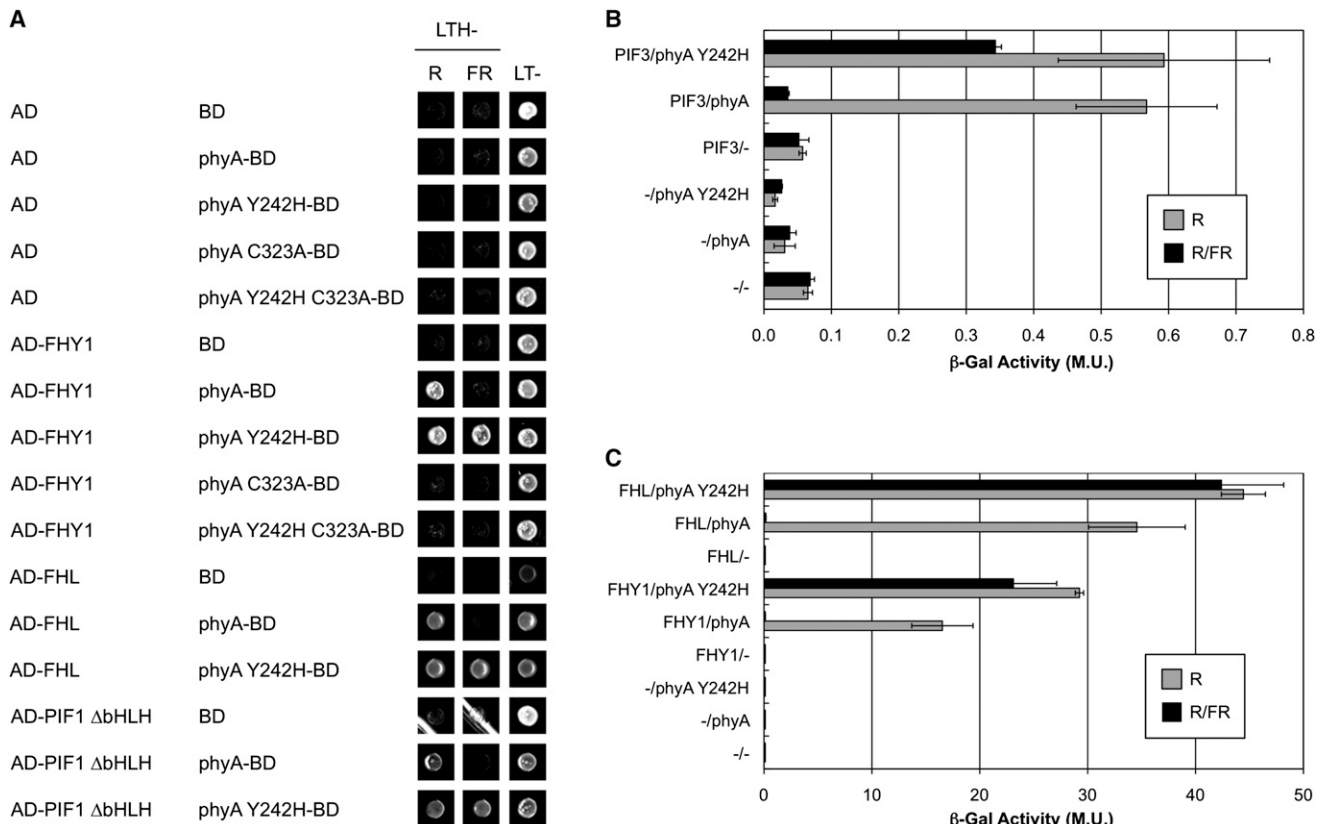


**Figure 2. Constitutive Interaction of PhyA Y242H and FHY1/FHL**

(A) PhyA Y242H constitutively interacts with FHY1, FHL, and PIF1. Yeast cells coexpressing the indicated plasmid constructs were grown on nonselective plates (CSM LT-) or on selective plates (CSM LTH-) supplemented with 1 mM 3-AT and 10  $\mu$ M PCB (phycocyanobilin). The selective plates were incubated in FR (15  $\mu$ mol  $m^{-2} s^{-1}$ ) or R (1  $\mu$ mol  $m^{-2} s^{-1}$ ) to convert phyA to Pr and Pfr, respectively. AD, GAL4 activation domain; BD, GAL4 DNA-binding domain.

(B) PhyA Y242H constitutively interacts with PIF3. Yeast cells transformed with the indicated plasmids were used for an ONPG assay. The yeast cultures were irradiated for 5 min with R (15  $\mu$ mol  $m^{-2} s^{-1}$ ), either followed by a 5 min FR (15  $\mu$ mol  $m^{-2} s^{-1}$ ) treatment (R/FR) or not (R), and were incubated for another 4 hr before measuring the  $\beta$ -Gal activity.  $n = 3$ . Error bars represent SEM.

(C) PhyA Y242H cannot be converted to Pr. Yeast cells were transformed with the indicated plasmids and used for an ONPG assay as described in (B).  $n = 3$ . Error bars indicate SEM.

See also Figure S2.

To study the qualitative behavior of the rescaled dynamic reaction scheme of Figure 4A and Figure S4B, we defined a list of input conditions, including the observations that FHY1/FHL protein levels positively correlate with the action of phyA and that expression of phyA Y242H-YFP reduces the hypocotyl length in dark-grown seedlings but interferes with hypocotyl growth inhibition in FR (Figure 4B). Although the list of input conditions includes the requirement that the simulated action spectrum exhibits a peak, we did not restrict its position to a specific wavelength. As output, we used the amount of nuclear-localized Pfr (= Pfrn). A systematic scan of the parameter space (Table S1) found those combinations, which reproduced all of the input conditions, defining the “admissible parameter space” of the problem posed. Among  $10^6$  randomly chosen parameter sets, we found 6050 admissible parameter combinations ( $\sim 1$  in 165), for each of which we simulated an action spectrum between 640 and 720 nm. Surprisingly, almost all admissible combinations resulted in an action spectrum with a peak in FR (Figures 5A and

5B). Hence, the underlying structure of the dynamic model and the input conditions defined in Figure 4B result in an obligate shift of the action peak to FR as seen for the HIR (Hartmann, 1967; Shinomura et al., 2000; Dieterle et al., 2001) (Figure S1).

Efficient phyA nuclear accumulation requires continuous irradiation with FR despite maximal Pfr abundance in R, which reflects the distinctive features of the HIR (Kim et al., 2000). Thus, the crucial test for the theoretical description of the phyA dynamics is whether the model correctly predicts the nuclear abundance of phyA in R and FR. A simulation revealed that, for 92% of all admissible parameter combinations (total 5566,  $\sim 1$  in 179), the total amount of phyA accumulating in the nucleus was higher at 720 nm than at 660 nm.

### Sensitivity Analysis

To study the sensitivity to variations of individual parameters, we took the remaining 5566 admissible parameter combinations and varied one parameter value at a time while holding all of

the others fixed (see [Supplemental Information](#)). The position of the action peak was mainly influenced by the Pfr-FHY1 complex dissociation rate, followed by the Pfr degradation rate ([Figure 5C](#)). Decreasing the Pfr degradation rate shifted the position of maximal activity to shorter wavelengths ([Figure S5A](#)), whereas the shift of the peak due to variation of the Pfr-FHY1 complex dissociation rate is not uniform throughout the admissible parameter space ([Figure S5B](#); see [Supplemental Information](#)). Varying the other parameters only weakly influenced the peak position. Considering the peak height, we found that the total amount of FHY1 and FHL ( $f_0$ ), as well as the Pfr degradation rate, were the most crucial parameters affecting the amount of nuclear-localized Pfr ([Figure 5D](#)). Decreasing the Pfr degradation rate increased the peak height ([Figure S5C](#)). It has been shown that FHY1/FHL-overexpressing seedlings are hypersensitive to FR, whereas *fhy1* and *fhy1 fhl* mutant plants are hyposensitive ([Desnos et al., 2001](#); [Whitelam et al., 1993](#); [Zhou et al., 2005](#)). Variation of the parameter  $f_0$  affected the peak height in a way that is consistent with these reports ([Figure S5D](#)). For all other parameters, we found a rather low sensitivity with respect to the height of the action peak. Note that the sensitivities of peak height and position are mostly nuclear specific (insets [Figures 5C](#) and [5D](#); see [Supplemental Information](#)).

### Experimental Verification of Model Predictions

According to the model's predictions, inserting a nuclear localization signal (NLS) into phyA Y242H-YFP or increasing the FHY1 levels in phyA Y242H-YFP-expressing plants should result in completely light-independent signaling ([Table S2](#); see [Supplemental Information](#)). To validate the predictive power of the model, we verified these key predictions experimentally by generating transgenic seedlings expressing phyA Y242H-NLS-YFP or phyA Y242H-YFP in the presence of 35S promoter-driven CFP-FHY1.

Although phyA Y242H-NLS-YFP was present at very low levels, it induced a strong *cop* phenotype in dark-grown Col-0 and *phyA* seedlings ([Figure 6A](#)). Moreover, FR-grown Col-0 seedlings expressing phyA Y242H-NLS-YFP were indistinguishable from the wild-type, suggesting that inserting a NLS into phyA Y242H-YFP is sufficient to suppress its dominant-negative effect. Overexpression of FHY1 in phyA Y242H-YFP-containing plants resulted in a strong *cop* phenotype as well ([Figure 6D](#)). In accordance with the idea that phyA Y242H-YFP interferes with FHY1 recycling, we found that increasing the FHY1 levels strongly promotes nuclear accumulation of phyA Y242H-YFP ([Figure 6E](#)).

To demonstrate that inserting a NLS into phyA Y242H-YFP specifically overcomes defects in nuclear transport, but not in downstream signaling, we crossed Col-0  $P_{PHYA}:PHYA$  Y242H-NLS-YFP seedlings into the *hy5* mutant, which is defective in transduction of light signals ([Oyama et al., 1997](#)). Irrespective of whether grown in D (dark) or FR, *hy5*  $P_{PHYA}:PHYA$  Y242H-NLS-YFP seedlings had much longer hypocotyls than the parent line expressing the same construct in wild-type background ([Figure 6B](#)). Microscopy studies confirmed the nuclear localization of phyA Y242H-NLS-YFP in both Col-0 and *hy5* seedlings ([Figure S6A](#)).

When grown on medium supplemented with sucrose seedlings expressing phyA Y242H-NLS-YFP continued photomorphogenic growth in complete darkness, developed leaves, and

started to flower after 6 weeks ([Figure 6C](#) and [Figures S6B–S6D](#)). Under these conditions, other photoreceptors (phyB–E, cryptochromes, phototropins, UV-B receptors) are inactive, suggesting that phyA is sufficient for the development from seeds to flowering plants.

### Unraveling the Core Mechanisms for Shifting the Action Peak to FR

In the previous sections, we have shown that our model ([Figure 4A](#)) for the phyA dynamics is capable of reproducing the observed wavelength shift in the action spectrum and that this property prevails in most of the admissible parameter space defined by the input conditions given in [Figure 4B](#). To identify the core mechanism being responsible for the wavelength shift, we adopted an abstract viewpoint on the phyA dynamics. We constructed networks using the key property of phytochromes—namely, their capability of interconversion between different states via light absorption. A generic network consists of vertexes, i.e., different states, and edges, i.e., transitions between the states. The edges can be light regulated—like the transition between Pr and Pfr—or light independent. Because we singled out a state as being the effector for further downstream signaling, we considered the direction from the influx into the network, i.e., synthesis, to the effector as being the forward direction. Therefore, we distinguished between two types of light-dependent edges. Type I consists of the light-induced transition from a state X to a different state Y at rate of the Pr→Pfr transition ( $k_1$ ) and the back transition from Y to X with rate of the Pfr→Pr conversion ( $k_2$ ). Type II represents the reversed edge, i.e., light-induced transition from X to Y at rate  $k_2$  and the back transition from Y to X at rate  $k_1$  ([Figure 7A](#)). This means that the forward directions of the edges exhibit the wavelength characteristics of the Pr form (type I) and the Pfr form (type II), with maxima at 667 nm and 730 nm, respectively. In addition, light-independent transitions between states (type 0 edges; e.g., biochemical reactions or transport events) could occur as well as synthesis and degradation at the vertexes. For simplicity, we considered synthesis or influx into the network only at one vertex, which is attached to a type I edge. This reflects that phytochromes are synthesized in the Pr state and activated by the light-induced transition to Pfr. Moreover, we considered the wavelength-dependent abundance of the effector as the action spectrum of the network.

The simplest network that one can construct with the elements summarized in [Figure 7A](#) is the network with influx into state X connected to Y by an edge of type I ([Figure 7B](#)). This represents the phytochrome reaction network in which X is the Pr and Y the Pfr form ([Schäfer and Mohr, 1974](#)). The corresponding action spectra given by the abundance of Y are shown in [Figure 7B](#). For low fluence rates (see [Supplemental Information](#)), the action spectrum resembled the Pr absorption spectrum ([Mancinelli, 1994](#)), whereas it became virtually independent of the wavelength for high fluence rates, approaching the photo-equilibrium. The position of the maxima was almost independent of the parameters and coincided with the position of the Pr absorption maximum ([Mancinelli, 1994](#)), which was expected for this simple network. To obtain a network exhibiting maximal response in FR instead of R, we proceeded by adding an edge of type II, the

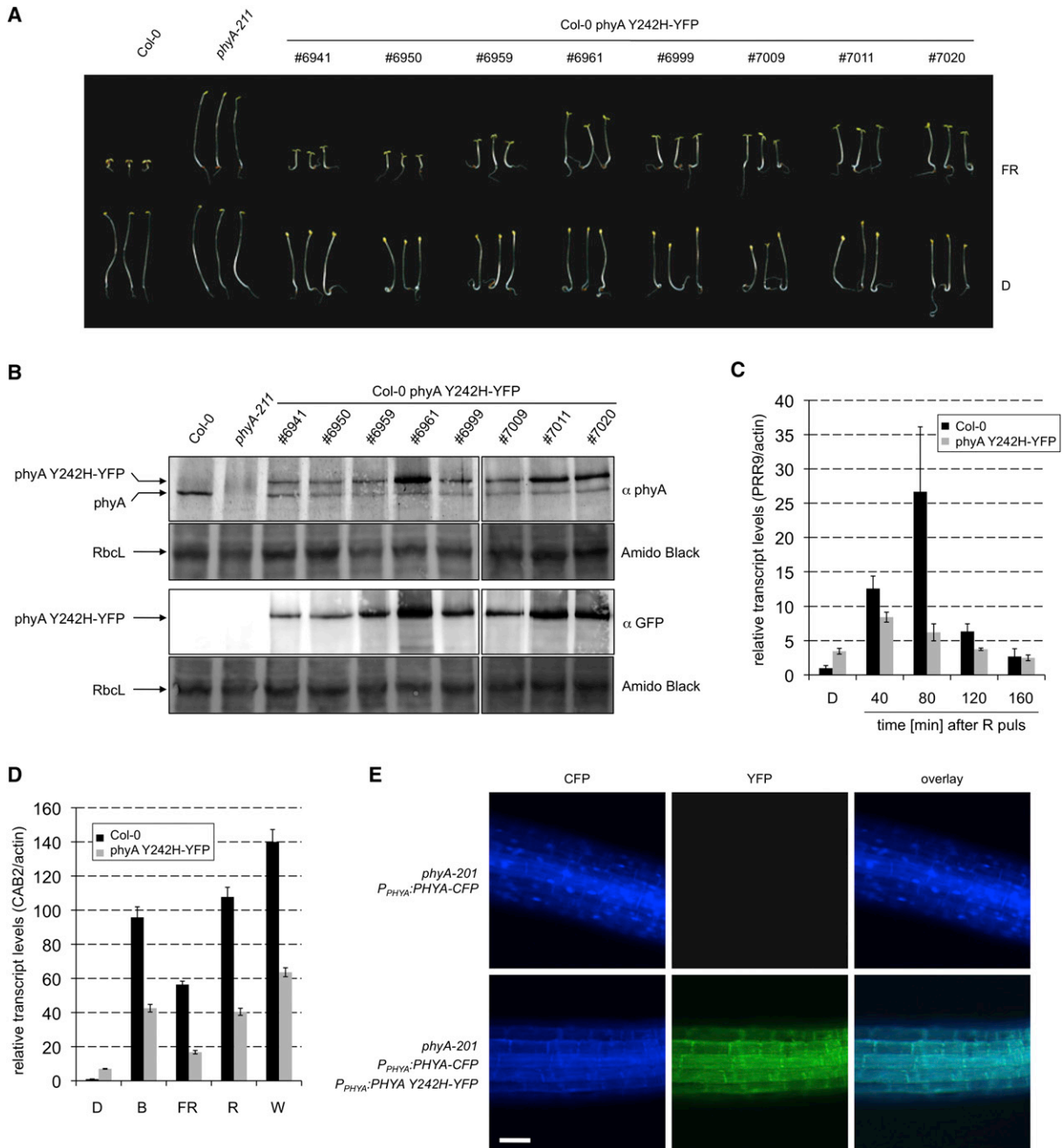


**Figure 3. The PhyA Y242H-YFP Phenotype**

(A) Expression of phyA Y242H-YFP interferes with FR perception. Wild-type (*Arabidopsis* Col-0), as well as several independent transgenic lines expressing  $P_{PHYA}$ :PHYA Y242H-YFP in Col-0 background, were grown for 4 days in D (dark) or FR ( $15 \mu\text{mol m}^{-2} \text{s}^{-1}$ ).

(B) PhyA Y242H-YFP expression levels correlate with the strength of the phenotype. Fifteen  $\mu\text{g}$  of total protein isolated from 4-day-old dark-grown seedlings (Col-0, *phyA-211*, several independent lines expressing  $P_{PHYA}$ :PHYA Y242H-YFP in Col-0) were analyzed by immunoblotting with antibodies against phyA or GFP. A section of the amido black-stained membrane is shown as loading control.

(C) PRR9 transcript levels in phyA Y242H-YFP seedlings. Five-day-old, dark-grown Col-0 and Col-0  $P_{PHYA}$ :PHYA Y242H-YFP (line #6941) seedlings were irradiated for 30 s with R ( $0.042 \mu\text{mol m}^{-2} \text{s}^{-1}$ ) and were incubated for different time periods in D before RNA extraction. The transcript levels of PRR9 and ACTIN1 were determined by real-time RT-PCR. The expression levels of PRR9 were normalized to the levels of ACTIN1 (Col-0 in D was set to 1). Error bars represent SD.

(D) CAB2 transcript levels in phyA Y242H-YFP seedlings. Col-0 and Col-0  $P_{PHYA}$ :PHYA Y242H-YFP (line #6941) seedlings were grown for 4 days in D and either irradiated for 24 hr with B, FR, R, or W or incubated for another 24 hr in D before RNA extraction. Real-time RT-PCR analyses were done as described in (C). The expression levels of CAB2 were normalized to the levels of ACTIN1 (Col-0 in D was set to 1). Error bars represent SD.

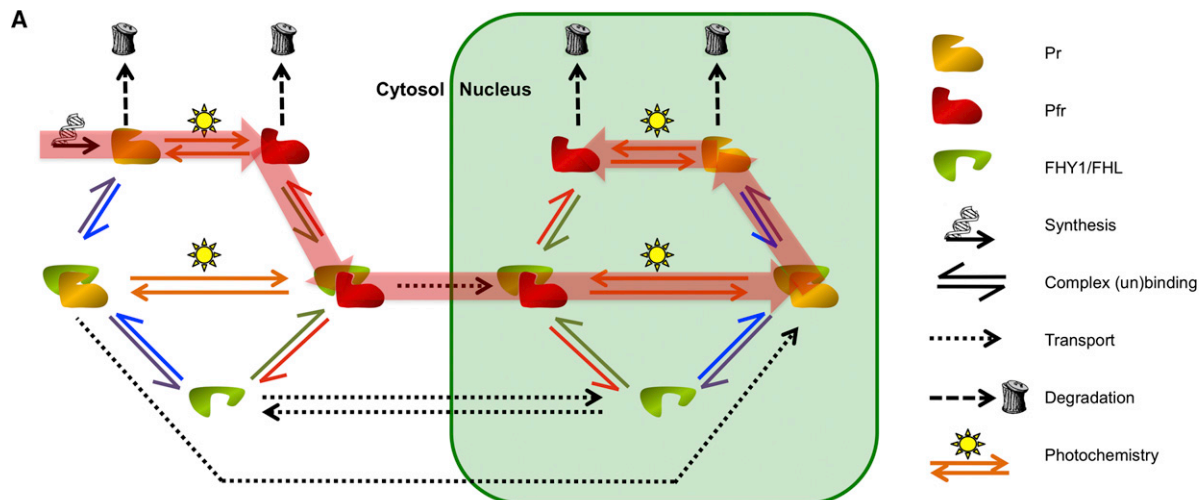


**Figure 4. PhyA Signaling Model and Input Conditions for the Parameter Scan**

(A) Dynamic model for phyA nuclear transport. See Figure S4B for parameter names. The HIR module (see text) is labeled in red.

(B) Experimental input conditions used for parameter scan.  $\text{phy}_{\text{nuc}}$ , nuclear-localized phytochrome (refer to Figure S5 for exact definition). cFR, continuous FR. See also Figure S4, Figure S5, and Table S1.

reversed light-dependent edge. For low fluence rates, the maximal response of the extended network is close to the Pr absorption maximum (which is reminiscent of the VLFR), whereas it is strongly shifted toward FR for high fluence rates (Figure 7C and Figure S7). Therefore, we discovered the smallest network (hereafter referred to as “HIR module” or “shifting module”) with an absorption maximum in R but exhibiting maximal response in FR under high irradiance conditions. Note that synthesis and degradation are absolutely essential ingredients that result in a constant particle flux through the network and render the system out of equilibrium. Thus, all explanations for the HIR based on equilibrium considerations are doomed to fail. The other essential ingredients, in addition to synthesis and degradation, are the type I and type II edges, which have

to occur pairwise in the pathway from the influx to the effector. They do not have to be linked directly to each other and may be separated by one or several type 0 edges. For an extended analysis and discussion, see the Supplemental Information.

There is a simple way to understand why the pair of type I/type II edges produces a shift in the action spectrum. The transition from  $\text{Pfr} \rightarrow \text{Pr}$  has its maximum in FR (Mancinelli, 1994), and hence it is essential to have a type II edge in forward direction, i.e., from synthesis to the signaling state. However, as phyA is synthesized in the Pr form, it first needs to be converted to Pfr, which requires a type I edge in forward direction. To have both transitions in forward direction in the pathway, it is indispensable that the initial Pr form and the final Pr form are different, i.e.,  $\text{Pr} \rightarrow \text{Pfr} \rightarrow \text{Pr}^*$ . How this can be achieved in planta is discussed in the

(E) PhyA Y242H-YFP inhibits nuclear accumulation of wild-type phyA. *PhyA-201*  $\text{P}_{\text{PHYA}}:\text{PHYA Y242H-YFP}$  was crossed into *phyA-201*  $\text{P}_{\text{PHYA}}:\text{PHYA-CFP}$  background. In the F2 generation, individuals homozygous for both transgenes were selected. Four-day-old dark-grown *phyA-201*  $\text{P}_{\text{PHYA}}:\text{PHYA-CFP}$  and *phyA-201*  $\text{P}_{\text{PHYA}}:\text{PHYA-CFP P}_{\text{PHYA}}:\text{PHYA Y242H-YFP}$  seedlings were irradiated with FR ( $15 \mu\text{mol m}^{-2} \text{s}^{-1}$ ) for 6 hr and were used for microscopy. Scale bar, 100  $\mu\text{m}$ .

See also Figure S3.

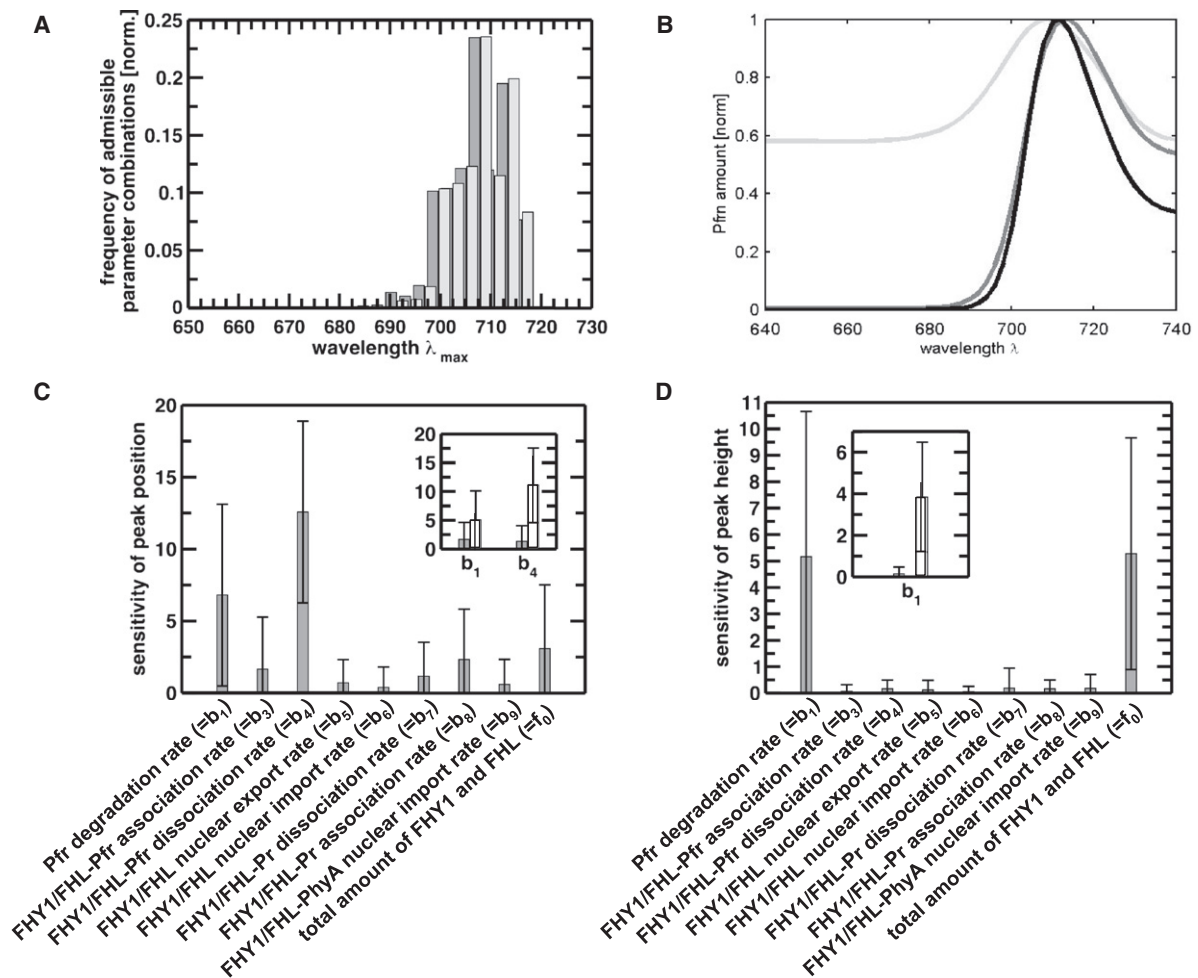


### Figure 5. Simulation Results

(A) Distributions of the admissible parameter combinations exhibiting maximal action at wavelength  $\lambda_{\max}$  when assuming the input conditions of Figure 4B (dark gray) or additionally assuming  $\text{phy}_{\text{nuc}}(660\text{nm}) < \text{phy}_{\text{nuc}}(720\text{nm})$  (light gray). The distributions were normalized to the total number of admissible parameters.

(B) Representative action spectra (for three arbitrary admissible parameter combinations) based on the relative and saturated amount of Pfr in FR irradiation. (C and D) Parameter sensitivity of the dynamic constants with respect to the peak position (C) and the peak height (D). The insets show the contributions from the cytosolic (gray) and the nuclear (white) parameter variations. Error bars represent SD.

See also Figure S5 and Figure S7.

next section. Whether the wavelength characteristic of the Pr  $\rightarrow$  Pfr transition (peak at 667 nm) or the Pfr  $\rightarrow$  Pr transition (peak at 730 nm) dominates depends on the degradation rates and the light intensity (see Supplemental Information). It is important to note that, in order to obtain the shift of the action peak from R to FR, the degradation rate of the intermediate state (Y in Figure 7C) needs to be higher than that of the initial state (X in Figure 7C; see Supplemental Information). Thus, it follows that, in a realistic phyA network, the stability of the intermediate Pfr state has to be reduced compared to the stability of the Pr state, which is in accordance with experimental data (Hennig et al., 2000).

To investigate the effect of having more than one HIR module, we concatenated several modules, with influx into the first module and state Z of the last module being the effector (Figure 7D). The serial connection of wavelength-shifting modules resulted in sharpening of the peak, which, in planta, may be

important to better separate the action of phyA from that of other phytochromes (e.g., phyB) having an action peak in R. Using measured data (Dieterle et al., 2001), we estimated that the shift and the observed narrow range of the phyA action spectrum in planta is achieved by concatenating three to four shifting modules (see Supplemental Information).

### Network Realization In Planta

Using an abstract viewpoint, we unraveled the essential building elements to construct a network with an absorption maximum in R but maximal response in FR. In Figures 7E–7G, we suggest three different possibilities of how such a network can be realized in planta. The first one is that, upon binding to a kinase, phyA is phosphorylated (Figure 7E). It is important that the kinase dominantly and strongly binds to Pfr. This ensures that the reversed light-induced transformation is indispensable to release

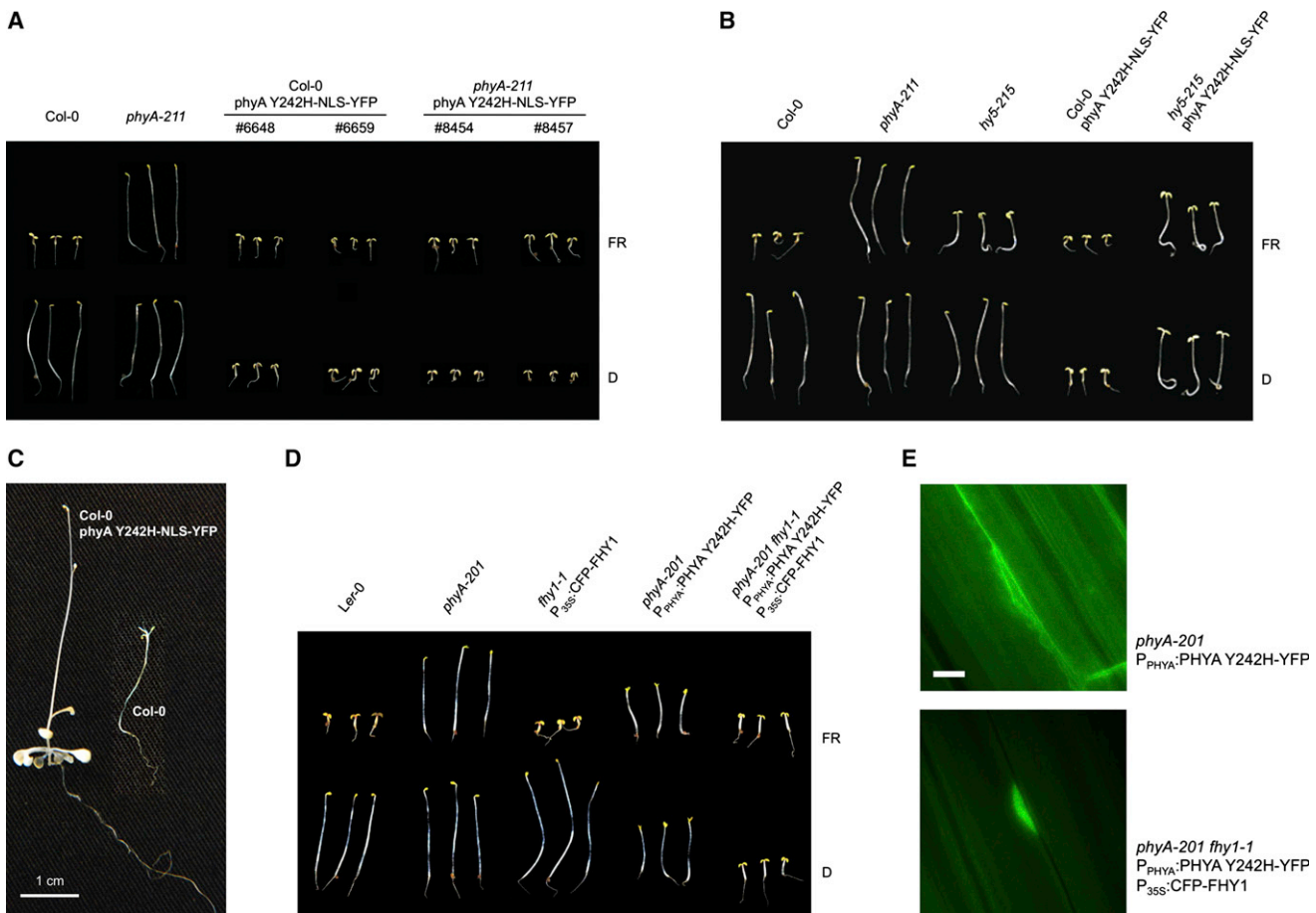


**Figure 6. PhyA Y242H-NLS-YFP Seedlings Exhibit a *cop* Phenotype**

(A) Targeting phyA Y242H-YFP to the nucleus results in a *cop* phenotype. Wild-type (*Arabidopsis* Col-0) and *phyA-211* seedlings, as well as independent transgenic lines expressing P<sub>PHYA</sub>:PHYA Y242H-NLS-YFP in Col-0 or *phyA-211* background, were grown for 4 days in D or FR ( $15 \mu\text{mol m}^{-2} \text{s}^{-1}$ ).

(B) The *hy5* mutant reduces the *cop* phenotype of phyA Y242H-NLS-YFP-expressing lines. Col-0 P<sub>PHYA</sub>:PHYA Y242H-NLS-YFP (line #6648) was crossed into *hy5-215* mutant background. Col-0, *phyA-211*, and *hy5-215* seedlings, as well as transgenic lines expressing P<sub>PHYA</sub>:PHYA Y242H-NLS-YFP in Col-0 or *hy5-215* background, were grown for 4 days in D or FR ( $15 \mu\text{mol m}^{-2} \text{s}^{-1}$ ).

(C) PhyA Y242H-NLS-YFP-expressing plants flower in D. Col-0 plants expressing P<sub>PHYA</sub>:PHYA Y242H-NLS-YFP were grown for 6 weeks in the dark on 1/2 × MS, 0.7% agar supplemented with 1% sucrose.

(D) Overexpression of FHY1 induces a strong *cop* phenotype in phyA Y242H-YFP seedlings. *PhyA-201* seedlings expressing P<sub>PHYA</sub>:PHYA Y242H-YFP were crossed into *fhy1-1* P<sub>35S</sub>:CFP-FHY1 background. A line that is homozygous for the *phyA-201* and *fhy1-1* mutations, as well as for both transgenes, was selected and grown for 4 days in D or FR ( $15 \mu\text{mol m}^{-2} \text{s}^{-1}$ ). The respective parent lines, as well as wild-type (*Arabidopsis* Ler-0), *phyA-201*, and *fhy1-1* seedlings, were grown under the same conditions.

(E) PhyA Y242H-YFP accumulates in the nucleus of FHY1-overexpressing lines. *PhyA-201* P<sub>PHYA</sub>:PHYA Y242H-YFP and *phyA-201 fhy1-1* P<sub>PHYA</sub>:PHYA-YFP P<sub>35S</sub>:CFP-FHY1 seedlings were grown for 4 days in D and were used for microscopic analysis. Only the YFP channel is shown. Scale bar, 5  $\mu\text{m}$ .

See also Figure S6.

phosphorylated phyA, which is considered to be the effector. Alternatively, phyA interacts with another protein (C), which is subsequently marked (Figure 7F). The marked form of this protein is the active form for further downstream signaling. Again, it is important that the interacting protein C dominantly binds to Pfr. Finally, the network with the pair of type I/type II edges can also be realized using different compartments (Figure 7G). Here, Pfr strongly binds to a transport protein and is released after the light-induced back transformation to Pr. Note that, in all three examples, the Pfr complex dissociation rate needs to be significantly lower than  $k_2$ , the rate of Pfr → Pr

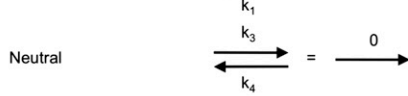
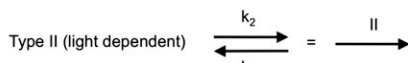
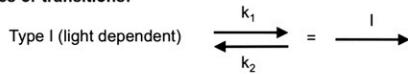
photoconversion, and the stability of the Pfr complex must be higher than that of the Pr complex. Otherwise the type II edge, i.e., the light-induced conversion of Pfr → Pr, would not be necessary, and the HIR module would be lost.

The network presented in Figure 4A predominantly produces action spectra with peaks shifted toward FR. Comparing the signaling network shown in Figure 4A with the shifting modules presented in Figures 7E–7G reveals that, in the phyA-signaling network, the shifting module is realized using different compartments (Figures 7G and 7H; highlighted in Figure 4A). Thus, in planta, the pair of type I/type II edges is represented by the

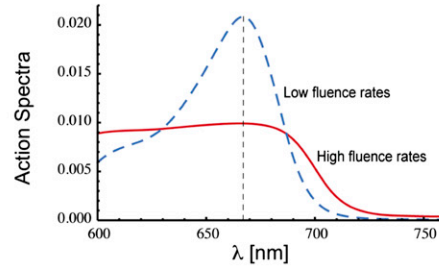
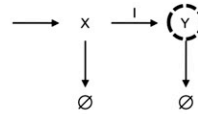
**A Vertices or states:**

X, Y, Z

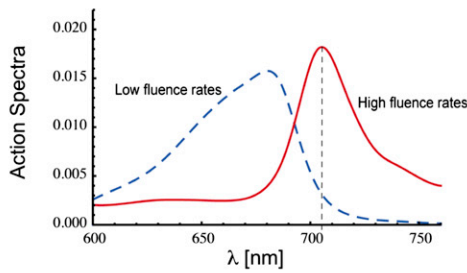
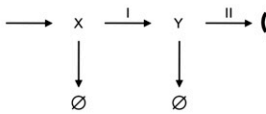
**Edges or transitions:**



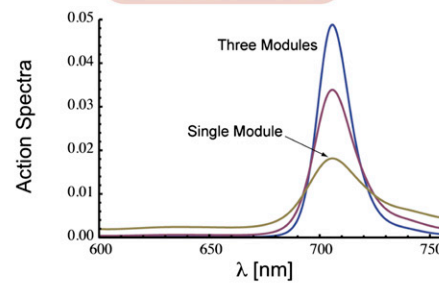
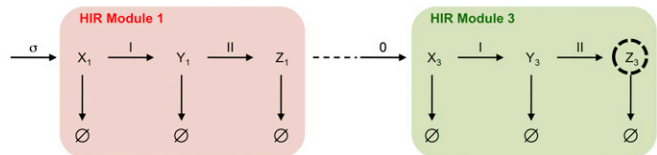
**B**



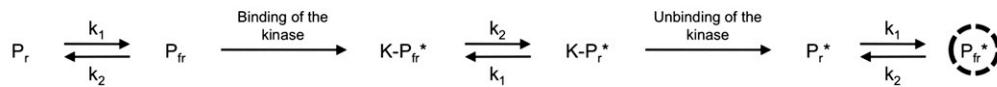
**C**



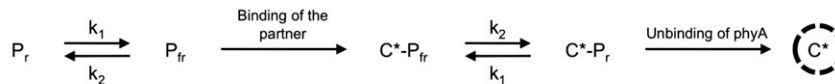
**D**



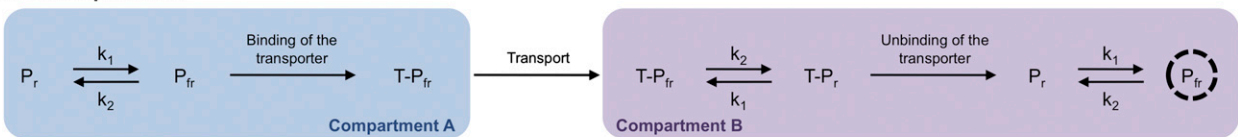
**E Phosphorylation of phyA**



**F Phosphorylation of an interaction partner**



**G Different compartments**



**H FHY1/FHL-dependent nuclear transport**

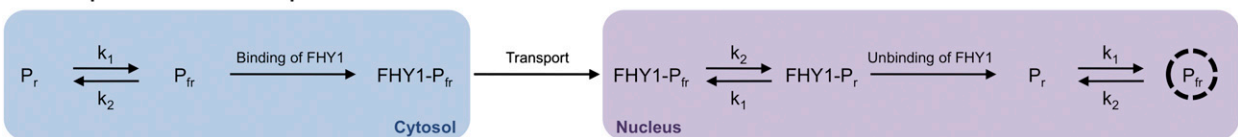


**Figure 7. The Shifting Module**

(A–D) Constructing a simple wavelength-shifting network.  
 (A) Basic construction elements.

cytosolic and nuclear photoconversion cycles, which operate in opposite directions. As both photoconversion cycles are essential to generate the shift of the action peak from R to FR, the FHY1-Pfr complex dissociation rate needs to be lower than the rate of Pfr→Pr photoconversion, and the FHY1-Pfr complex has to be more stable than the FHY1-Pr complex. Consistent with these requirements, yeast two-hybrid and in vitro pull-down assays support the idea that FHY1-Pfr complexes are more stable than FHY1-Pr complexes (Hiltbrunner et al., 2005, 2006; Sorokina et al., 2009). However, despite the fact that the Pfr/Ptot ratio is roughly 40-fold higher in R than FR, the amount of FHY1-phyA complexes in planta is higher in FR than in R, i.e., under conditions in which the Pfr/Ptot ratio is very low (Shen et al., 2009; Yang et al., 2009). Yet, our model is in agreement with this counterintuitive result. When we analyzed the relative levels of FHY1-phyA complexes, we found that, for 79% of the admissible parameters, the relative amount of FHY1-phyA complexes is higher at 726 nm (FR) than at 660 nm (R) (Figure S7C).

## DISCUSSION

### Three Cycles to Explain phyA Nuclear Accumulation

The core structure of our model for light- and FHY1/FHL-dependent phyA nuclear transport consists of a cytosolic and a nuclear-localized Pr/Pfr photoconversion cycle and an FHY1/FHL-Pr/Pfr complex association/dissociation cycle, which links the two photoconversion cycles (Figure S4 and Figure 4A). In this report, we suggest that photocycling between Pr and Pfr per se is essential for responsiveness to FR. Consistent with this notion, phyA mutant versions, which are constitutively in Pfr- or Pr-like states (i.e., phyA Y242H and phyA C323A), cannot substitute for wild-type phyA, which continuously cycles between Pr and Pfr when irradiated with light. It was shown that phyA-FHY1/FHL complexes rapidly dissociate after conversion of Pfr to Pr (Genoud et al., 2008; Sorokina et al., 2009). Thus, photocycling between Pr and Pfr results in continuous assembly and disassembly of phyA-FHY1/FHL complexes. Successive cycles of binding to FHY1/FHL in the cytosol and dissociation of phyA-FHY1/FHL transport complexes in the nucleus after photoconversion of Pfr to Pr would lead to nuclear accumulation of phyA. One concern with this model is that the half-life of Pfr-FHY1/FHL complexes may not be long enough to complete transport through the nuclear pore before photoconversion of Pfr to Pr results in dissociation of the complexes. However, active transport of NLS-containing proteins or protein complexes across the nuclear membrane requires 10–20 ms, whereas even in high fluence rate FR, the half-life of Pfr is roughly

three orders of magnitude longer (Frey and Görlich, 2007; Mancinelli, 1994). Importantly, this model also offers an explanation for the fluence rate dependence of phyA nuclear transport. The rate of photocycling is proportional to the fluence rate, i.e., light intensity (Mancinelli, 1994). Thus, high light intensities (at least in the range occurring under natural conditions) would increase the transport capacity by increasing the rate of FHY1/FHL-phyA complex assembly and disassembly.

### Toward Understanding the HIR in Molecular and Mathematical Terms

Although the Pfr/Ptot ratio is highest in R, phyA-mediated responses are most efficiently triggered by FR, in which the Pfr/tot ratio is roughly 40-fold lower than in R. PhyA is unique to higher plants and enables them to de-etiolate in shady habitats, which are characterized by a high FR content. As such, phyA may have provided an adaptive advantage to angiosperms, promoting their rapid radiation in the mid-Cretaceous (Mathews, 2005). The shift from maximal absorption in R to maximal activity in FR (Figure S1) has been known for more than half of a century (Mohr, 1957) but could not be linked to defined components or molecular events so far.

The mathematical model presented here integrates the current knowledge on phyA nuclear transport and degradation into a dynamic interaction network. A systematic sampling of the parameter space found the admissible parameter combinations for which the model in Figure 4A reproduced a list of input conditions, including the existence of a peak in the action spectrum. Although the position of the peak was not defined in the list of input conditions, the simulated action spectra exhibited a peak in FR throughout the admissible parameter space (Figure 5). Moreover, for almost all admissible parameter combinations, the total amount of phyA in the nucleus was maximal in FR. Therefore, the shift of the peak in the action spectrum from R to FR, as well as maximal nuclear accumulation of phyA in FR, are intrinsic features of our model (Figure 4A and Figure S4).

### Defining the “HIR Module”

Our investigation of small light-regulated networks revealed the fundamental structural requirements for the HIR: nonequilibrium, i.e., synthesis and degradation, and a pair of reversed light-dependent edges in the pathway from synthesis to the effector.

Consistent with the scenario in Figure 7G, our model for phyA nuclear transport contains a pair of spatially separated, reversed light-dependent edges, i.e., the cytosolic and nuclear Pr/Pfr photoconversion cycles, which operate in opposite directions (Figure 4A, Figure 7H, and Figure S4). As both cycles are required to generate the shift of maximal action from R to FR, the

(B) Network reflecting the usual phytochrome reaction network.

(C) Response shifting/HIR module. The position of the action peak is fluence rate dependent and for high fluence rates in the FR region of the spectrum.

(D) Serial connection of several HIR modules. Concatenating multiple HIR modules leads to sharpening of the action peak.

(E–H) Possible network realization in planta.

(E) Binding of a kinase results in a phosphorylated phyA, which is the effector.

(F) Phosphorylation of a binding partner, which is the effector.

(G) Binding of a transporter, which transports phyA into a different compartment, where it acts as the effector.

(H) HIR module realized in planta.

See also Figure S7.

FHY1-Pfr complex dissociation rate has to be lower than  $k_2$ , the rate of Pfr→Pr photoconversion, and the stability of the Pfr-FHY1 complex needs to be higher than that of the Pr-FHY1 complex. Bypassing the need of the Pfr→Pr photoconversion cycle in the nucleus by having an FHY1-Pfr complex dissociation rate higher than  $k_2$  and/or a lower stability of the Pfr-FHY1 than the Pr-FHY1 complex would result in a loss of the HIR module.

Importantly, our analysis also revealed that phyA degradation is essential not only to prevent excessive signaling and interference with the shade avoidance response (Debrieux and Fankhauser, 2010), but also to obtain a maximal response in FR.

### “Ecological” Relevance and Evolution of the HIR

PhyA is the most abundant phytochrome species in etiolated seedlings, whereas phyB dominates in plants grown in light. It has been hypothesized that degradation of phyA in R is important to clearly separate between the action of phyA and phyB. An alternative way to increase the specificity between phyA and phyB is to sharpen the peaks of their action spectra in order to minimize the overlap. For phyA, this can be achieved by concatenating several HIR modules, as shown in Figure 7D. Based on our theoretical analysis, we estimate the number of HIR modules in planta to be three to four. So far, we discovered one of these modules, the FHY1 import cycle. It is well established that phyA nuclear transport is a prerequisite for FR perception and that it works most efficiently under HIR conditions (Hiltbrunner et al., 2006; Kim et al., 2000; Rösler et al., 2007). These findings are consistent with the idea that the FHY1 import cycle is one of the HIR modules. In line with our estimate, there is strong experimental evidence for the existence of additional HIR modules. Fusing a NLS directly to phyA bypasses the FHY1 import cycle (i.e., the “first” HIR module) and, as a consequence, should result in a loss of the R→FR shift of the action peak. Yet, phyA localizing constitutively to the nucleus perfectly responds to FR, and expression of phyA-NLS restores sensitivity to FR in the absence of FHY1 (Genoud et al., 2008). This strongly argues for the existence of at least one additional HIR module acting in the nucleus (i.e., downstream of phyA nuclear transport).

Light filtering through the foliage of forest trees is depleted of photosynthetically active radiation (mainly B and R) and is strongly enriched in FR. The colonization of understory areas has been associated with the emergence of a photoreceptor system that is able to perceive FR (Mathews, 2005). Data presented in this report suggest that higher plants acquired such a FR sensing system by using a photoreceptor with maximal absorption in R and adjusting its molecular interactions rather than changing the photophysical properties of the photoreceptor itself. The Pr and Pfr absorption spectra of phyA and phyB are virtually identical, whereas the action spectra differ dramatically, with phyA having an action peak in FR and phyB in R (Eichenberg et al., 2000; Hartmann, 1967; Shinomura et al., 1996, 2000). Two main differences between phyA and phyB are the Pfr degradation rate and the mechanism employed for nuclear transport. Whereas phyA is rapidly degraded in Pfr, phyB is much more stable and, in contrast to phyA, does not depend on FHY1/FHL for nuclear transport (Bae and Choi, 2008; Hiltbrunner et al., 2006). Strong Pfr degradation and the FHY1/FHL transport cycle

are essential components of the HIR module that we identified. Increasing the Pfr degradation rate of phyB and rendering its nuclear transport FHY1/FHL dependent may therefore result in a shift of its action peak toward FR. Currently, the amino acid residues that are responsible for the different behavior of phyA and phyB regarding Pfr stability and nuclear transport are unknown. However, once these residues have been identified, it seems feasible to recapitulate the evolution of the phyA-based FR sensing system that is present in today’s plants by changing the respective residues in phyB and shifting its action peak to FR.

### Conclusion

Previous models for the HIR assumed that neither dark-synthesized Pr nor photoconverted Pfr is the phyA species mediating the HIR but that it has to be modified in some way (Schäfer et al., 1975; Shinomura et al., 2000). Data presented in this report suggest that nuclear-localized Pfr is active in signaling (Figure 6) but that photocycling between Pr and Pfr is essential to shift the peak in the action spectrum from R to FR. This is consistent with the idea by Shinomura et al. (2000) that the HIR depends on photocycling of phyA. However, the strength of our model is that it provides an explanation in molecular and mathematical terms of why photocycling is essential for phyA nuclear transport and HIR signaling.

### EXPERIMENTAL PROCEDURES

#### Fluorescence Microscopy and FRAP/FLIP Analyses

Fluorescence microscopy was done as described (Hiltbrunner et al., 2006). Three-day-old etiolated seedlings expressing P<sub>35S</sub>:YFP-FHY1 in either *thy1-1* or *phyA-201* background were used to perform FRAP and FLIP assays as described in the Extended Experimental Procedures.

#### Plasmid Constructs and Plant Material

A detailed description of the plasmid construct used in this study can be found in the Extended Experimental Procedures. The *phyA-201* (= *fre-1*) and *thy1-1* mutants (in *Ler*), as well as the *phyA-211*, *thy1-3* (= *pat3*), *thl-1*, and *hy5-215* mutants (in *Col*) have been described (Desnos et al., 2001; Oyama et al., 1997; Quail et al., 1994; Whitelam et al., 1993; Zeidler et al., 2001; Zhou et al., 2005). *Col-0* and *Ler-0* were used as wild-type.

The *thy1-3 thl-1* double mutant was obtained by crossing the respective single mutants. The transgenic lines expressing P<sub>35S</sub>:YFP-FHY1 (*thy1-1* pCHF70-FHY1) and P<sub>PHYA</sub>:PHYA-CFP (*phyA-201* pphyA40-phyA) have been described (Genoud et al., 2008; Hiltbrunner et al., 2005). All other lines were obtained by Agrobacterium-mediated transformation or by crossing pre-existing lines, as described in the Extended Experimental Procedures. For details regarding growth conditions, refer to the Extended Experimental Procedures.

#### Yeast Two-Hybrid Assays, Immunoblot Analyses, and qPCR

Yeast two-hybrid growth and ONPG assays and immunoblot analyses were done as described (Genoud et al., 2008; Hiltbrunner et al., 2006). The antibody against phyA has been described in Hiltbrunner et al. (2006). Antibodies specific for green fluorescent protein (GFP)/YFP/CFP were purchased from Covance (Princeton, NJ, USA). qPCR was done according to standard protocols using gene-specific primers and probes for PRR9, CAB2, and ACTIN1. See the Extended Experimental Procedures for details.

### SUPPLEMENTAL INFORMATION

Supplemental Information includes Extended Experimental Procedures, seven figures, and three tables and can be found with this article online at doi:10.1016/j.cell.2011.07.023.

## ACKNOWLEDGMENTS

We are grateful to Dr. M. Zeidler and the ABRC for providing *thy1-3* and *fhl-1* seeds. We thank Prof. J. Paszkowski for the kind gift of the pWCO35 plasmid, Dr. S. Kircher for support for FRAP/FLIP analyses, M. Krenz and C. König for technical assistance, and Prof. C. Fankhauser and Prof. R. Ulm for critically reading the manuscript. This work was supported by grants from the DFG to E.S. (SFB592) and to E.S. and J.T. (GRK1305, EXC294) and the BMBF-Freiburg Initiative in Systems Biology 0313921 (FRISYS) to C.F., J.T., and E.S.

Received: April 5, 2011

Revised: June 10, 2011

Accepted: July 13, 2011

Published: September 1, 2011

## REFERENCES

- Bae, G., and Choi, G. (2008). Decoding of light signals by plant phytochromes and their interacting proteins. *Annu. Rev. Plant Biol.* 59, 281–311.
- Casal, J.J., Luccioni, L.G., Oliverio, K.A., and Boccacandro, H.E. (2003). Light, phytochrome signalling and photomorphogenesis in *Arabidopsis*. *Photochem. Photobiol. Sci.* 2, 625–636.
- Clodong, S., Dühring, U., Kronk, L., Wilde, A., Axmann, I., Herzel, H., and Kollmann, M. (2007). Functioning and robustness of a bacterial circadian clock. *Mol. Syst. Biol.* 3, 90.
- Debrieux, D., and Fankhauser, C. (2010). Light-induced degradation of phyA is promoted by transfer of the photoreceptor into the nucleus. *Plant Mol. Biol.* 73, 687–695.
- Desnos, T., Puente, P., Whitelam, G.C., and Harberd, N.P. (2001). FHY1: a phytochrome A-specific signal transducer. *Genes Dev.* 15, 2980–2990.
- Devlin, P.F., Christie, J.M., and Terry, M.J. (2007). Many hands make light work. *J. Exp. Bot.* 58, 3071–3077.
- Dieterle, M., Zhou, Y.C., Schäfer, E., Funk, M., and Kretsch, T. (2001). EID1, an F-box protein involved in phytochrome A-specific light signaling. *Genes Dev.* 15, 939–944.
- Eichenberg, K., Bäurle, I., Paulo, N., Sharrock, R.A., Rüdiger, W., and Schäfer, E. (2000). *Arabidopsis* phytochromes C and E have different spectral characteristics from those of phytochromes A and B. *FEBS Lett.* 470, 107–112.
- Frey, S., and Görlich, D. (2007). A saturated FG-repeat hydrogel can reproduce the permeability properties of nuclear pore complexes. *Cell* 130, 512–523.
- Genoud, T., Schweizer, F., Tscheuschler, A., Debrieux, D., Casal, J.J., Schäfer, E., Hiltbrunner, A., and Fankhauser, C. (2008). FHY1 mediates nuclear import of the light-activated phytochrome A photoreceptor. *PLoS Genet.* 4, e1000143.
- Hartmann, K.M. (1967). [An action spectrum of photomorphogenesis under high energy conditions and its interpretation on the basis of phytochrome (hypocotyl growth inhibition in *Lactuca sativa* L)]. *Z. Naturforsch. B* 22, 1172–1175.
- Hennig, L., Büche, C., Eichenberg, K., and Schäfer, E. (1999). Dynamic properties of endogenous phytochrome A in *Arabidopsis* seedlings. *Plant Physiol.* 121, 571–577.
- Hennig, L., Büche, C., and Schäfer, E. (2000). Degradation of phytochrome A and the high irradiance response in *Arabidopsis*: a kinetic analysis. *Plant Cell Environ.* 23, 727–734.
- Hiltbrunner, A., Tscheuschler, A., Viczián, A., Kunkel, T., Kircher, S., and Schäfer, E. (2006). FHY1 and FHL act together to mediate nuclear accumulation of the phytochrome A photoreceptor. *Plant Cell Physiol.* 47, 1023–1034.
- Hiltbrunner, A., Viczián, A., Bury, E., Tscheuschler, A., Kircher, S., Tóth, R., Honsberger, A., Nagy, F., Fankhauser, C., and Schäfer, E. (2005). Nuclear accumulation of the phytochrome A photoreceptor requires FHY1. *Curr. Biol.* 15, 2125–2130.
- Hu, W., Su, Y.-S., and Lagarias, J.C. (2009). A light-independent allele of phytochrome B faithfully recapitulates photomorphogenic transcriptional networks. *Mol. Plant* 2, 166–182.
- Kim, L., Kircher, S., Toth, R., Adam, E., Schäfer, E., and Nagy, F. (2000). Light-induced nuclear import of phytochrome-A:GFP fusion proteins is differentially regulated in transgenic tobacco and *Arabidopsis*. *Plant J.* 22, 125–133.
- Mancinelli, A.L. (1994). The physiology of phytochrome action. In *Photomorphogenesis in Plants*, R.E. Kendrick and G.M.H. Kronenberg, eds. (Dordrecht: Kluwer Academic Publishers), pp. 211–269.
- Mathews, S. (2005). Phytochrome evolution in green and nongreen plants. *J. Hered.* 96, 197–204.
- Mohr, H. (1957). Der Einfluss monochromatischer Strahlung auf das Längenwachstum des Hypocotyls und auf die Anthocyanbildung bei Keimlingen von *Sinapis alba* L. (= *Brassica alba* Boiss.). *Planta* 49, 389–405.
- Oyama, T., Shimura, Y., and Okada, K. (1997). The *Arabidopsis* HY5 gene encodes a bZIP protein that regulates stimulus-induced development of root and hypocotyl. *Genes Dev.* 11, 2983–2995.
- Quail, P.H., Briggs, W.R., Chory, J., Hangarter, R.P., Harberd, N.P., Kendrick, R.E., Koornneef, M., Parks, B., Sharrock, R.A., Schäfer, E., et al. (1994). Spotlight on phytochrome nomenclature. *Plant Cell* 6, 468–471.
- Rockwell, N.C., Su, Y.S., and Lagarias, J.C. (2006). Phytochrome structure and signaling mechanisms. *Annu. Rev. Plant Biol.* 57, 837–858.
- Rösler, J., Klein, I., and Zeidler, M. (2007). *Arabidopsis* fhl/fhy1 double mutant reveals a distinct cytoplasmic action of phytochrome A. *Proc. Natl. Acad. Sci. USA* 104, 10737–10742.
- Schäfer, E. (1975). A new approach to explain the “high irradiance responses” of photomorphogenesis on the basis of phytochrome. *J. Math. Biol.* 2, 41–56.
- Schäfer, E., Lassig, T.U., and Schopfer, P. (1975). Photocontrol of phytochrome destruction in grass seedlings. The influence of wavelength and irradiance. *Photochem. Photobiol.* 22, 193–202.
- Schäfer, E., and Mohr, H. (1974). Irradiance dependency of the phytochrome system in cotyledons of mustard (*Sinapis alba* L.). *J. Math. Biol.* 1, 9–15.
- Shen, Y., Zhou, Z., Feng, S., Li, J., Tan-Wilson, A., Qu, L.J., Wang, H., and Deng, X.W. (2009). Phytochrome A mediates rapid red light-induced phosphorylation of *Arabidopsis* FAR-RED ELONGATED HYPOCOTYL1 in a low fluence response. *Plant Cell* 21, 494–506.
- Shinomura, T., Nagatani, A., Hanzawa, H., Kubota, M., Watanabe, M., and Furuya, M. (1996). Action spectra for phytochrome A- and B-specific photoinduction of seed germination in *Arabidopsis thaliana*. *Proc. Natl. Acad. Sci. USA* 93, 8129–8133.
- Shinomura, T., Uchida, K., and Furuya, M. (2000). Elementary processes of photoperception by phytochrome A for high-irradiance response of hypocotyl elongation in *Arabidopsis*. *Plant Physiol.* 122, 147–156.
- Sorokina, O., Kapus, A., Terecskei, K., Dixon, L.E., Kozma-Bognar, L., Nagy, F., and Millar, A.J. (2009). A switchable light-input, light-output system modelled and constructed in yeast. *J. Biol. Eng.* 3, 15.
- Su, Y.S., and Lagarias, J.C. (2007). Light-independent phytochrome signaling mediated by dominant GAF domain tyrosine mutants of *Arabidopsis* phytochromes in transgenic plants. *Plant Cell* 19, 2124–2139.
- von Dassow, G., Meir, E., Munro, E.M., and Odell, G.M. (2000). The segment polarity network is a robust developmental module. *Nature* 406, 188–192.
- Whitelam, G.C., Johnson, E., Peng, J., Carol, P., Anderson, M.L., Cowl, J.S., and Harberd, N.P. (1993). Phytochrome A null mutants of *Arabidopsis* display a wild-type phenotype in white light. *Plant Cell* 5, 757–768.
- Yang, S.W., Jang, I.C., Henriques, R., and Chua, N.H. (2009). FAR-RED ELONGATED HYPOCOTYL1 and FHY1-LIKE associate with the *Arabidopsis* transcription factors LAF1 and HFR1 to transmit phytochrome A signals for inhibition of hypocotyl elongation. *Plant Cell* 21, 1341–1359.
- Zeidler, M., Bolle, C., and Chua, N.-H. (2001). The phytochrome A specific signaling component PAT3 is a positive regulator of *Arabidopsis* photomorphogenesis. *Plant Cell Physiol.* 42, 1193–1200.
- Zhou, Q., Hare, P.D., Yang, S.W., Zeidler, M., Huang, L.-F., and Chua, N.-H. (2005). FHL is required for full phytochrome A signaling and shares overlapping functions with FHY1. *Plant J.* 43, 356–370.

## EXTENDED EXPERIMENTAL PROCEDURES

## FRAP/FLIP Analyses

Three-day-old, etiolated seedlings expressing  $P_{35S}$ :YFP-FHY1 in either *thy1-1* or *phyA-201* background were used to perform FRAP and FLIP assays (Cole et al., 1996; Tillemans et al., 2006). Confocal images were collected using a ZEISS-LSM-510-META-NLO microscope system and a C-Apochromat 63x/1.2W corr. objective. Pre-bleach and post-bleach images were taken using the 514 nm argon line at 75% output intensity and 0.9%–1% transmission (resolution 512 × 512, line average 4). For photobleaching 75% output intensity (514 nm argon line), 100% transmission and 25 iterations were used. The fluorescence was detected at 516–558 nm using HFT 458/514 Beam-Splitter. Each of the scanned image sections had a size of 71.4 × 71.4  $\mu\text{m}^2$ . For FRAP analyses single nuclei were defined as regions of interest. In each experiment, two pre-bleach images were collected. After photobleaching a series of 20 post-bleach images was acquired to record fluorescence recovery in the bleached nuclei. In addition, the fluorescence in non-bleached nuclei within the same image section was measured as a control. For FLIP experiments regions in the cytoplasm, which covered approximately half-length of the cell, were bleached. For one FLIP record set, two pre-bleach images were taken followed by a series of 23 photobleach/image scan cycles. Nuclei of non-bleached cells within the same image section were used as controls. The ZEISS LSM-5 software was used to measure the fluorescence in FRAP and FLIP assays. Data points in Figure 1 represent the mean of 6 independent measurements.

## Constructs

pphyA30-*phyA* C323A is a T-DNA vector containing a  $P_{PHYA}$ :PHYA C323A YFP- $\text{Ter}_{RbcS}$  cassette and *bar* as selectable marker (Block et al., 1987) and was obtained as follows. A *phyA* fragment containing the C323A mutation was PCR amplified from pBS II KS-*phyA* (Hiltbrunner et al., 2005) using 5' and 3' primers (ah013 and ah136; see Table S3 for primer sequences) including BamHI and MfeI sites. The C323A mutation was included in ah136. The PCR fragment was digested with BamHI-MfeI and ligated into pBS II KS-*phyA* cut with BamHI-MfeI to obtain pBS II KS-*phyA* C323A. The BamHI-EcoRV fragment from pBS II KS-*phyA* C323A was then ligated into pphyA30-*phyA* (Hiltbrunner et al., 2006) cut with BamHI-EcoRV to replace the wild-type fragment.

D153ah-*phyA* C323A is a yeast two hybrid vector containing *phyA* C323A-GAL4 BD. To obtain it *phyA* C323A was cut from pBS II KS-*phyA* C323A using BamHI-SpeI and ligated into the BamHI-SpeI site of D153ah-*phyA* (Hiltbrunner et al., 2006) to replace the wild-type *phyA*.

pphyA30-*phyA* Y242H is a T-DNA vector containing a  $P_{PHYA}$ :PHYA Y242H YFP- $\text{Ter}_{RbcS}$  cassette and *bar* as selectable marker and was obtained as follows. A *phyA* fragment containing the Y242H mutation was PCR amplified from pBS II KS-*phyA* (Hiltbrunner et al., 2005) using 5' and 3' primers (ah013 and ah281) including BamHI and NcoI sites. The Y242H mutation was included in ah281. The PCR fragment was digested with BamHI-NcoI and ligated into pphyA30-*phyA* (Hiltbrunner et al., 2006) cut with BamHI-BspHI to replace the wild-type fragment.

D153ah-*phyA* Y242H is a yeast two hybrid vector containing *phyA* Y242H-GAL4 BD, which was obtained as follows. A BamHI-AvrII fragment containing the Y242H mutation was cut from pphyA30-*phyA* Y242H and ligated into D153ah-*phyA* (Hiltbrunner et al., 2006) digested with BamHI-AvrII to replace the wild-type fragment.

D153ah-*phyA* Y242H C323A is a derivative of D153ah-*phyA* C323A. It was obtained by cutting a HindIII fragment from D153ah-*phyA* Y242H and ligating it in sense orientation into D153ah-*phyA* C323A cut with HindIII to replace the wild-type fragment.

pPPO30 is a T-DNA vector containing a  $P_{35S}$ -BamHI-XbaI-YFP- $\text{Ter}_{RbcS}$  cassette. As selectable marker pPPO30 and other pPPO vectors contain a mutant version of *PPO*, which confers resistance to Butafenacil (Hanin et al., 2001; Li et al., 2003). To obtain pPPO30 a Pvull-PstI fragment containing *PPO* was cut from pWCO35 (Hanin et al., 2001) and ligated into pCHF30 (Hiltbrunner et al., 2006) cut with PmlI-SbfI to replace *bar* as selectable marker.

pPPO30-*phyA* contains a  $P_{35S}$ :PHYA-YFP- $\text{Ter}_{RbcS}$  cassette and was obtained as follows. *phyA* was cut with BamHI-SpeI from pBS II KS-*phyA* (Hiltbrunner et al., 2005) and ligated into the BamHI-XbaI site of pPPO30.

pPPO30A-*phyA* is a derivative of pPPO30-*phyA* and contains a  $P_{PHYA}$ :PHYA-YFP- $\text{Ter}_{RbcS}$  cassette. The *phyA* promoter was cut with StuI-BamHI from pphyA30-*phyA* (Hiltbrunner et al., 2006) and ligated into the PmeI-BamHI site of pPPO30-*phyA* to replace the 35S promoter.

pPPO30A-*phyA* Y242H, a T-DNA vector containing a  $P_{PHYA}$ :PHYA Y242H-YFP- $\text{Ter}_{RbcS}$  cassette, was obtained as follows. Using BamHI-SpeI *phyA* Y242H was cut from D153ah-*phyA* Y242H and ligated into pPPO30 cut with BamHI-XbaI resulting in pPPO30-*phyA* Y242H. Then the 35S promoter in pPPO30-*phyA* Y242H was replaced with the *phyA* promoter as described for pPPO30A-*phyA*.

pPPO30A-*phyA* Y242H-NLS is a T-DNA vector containing a  $P_{PHYA}$ :PHYA Y242H-NLS-YFP- $\text{Ter}_{RbcS}$  cassette and was obtained as follows. A fragment coding for the C-terminal part of *phyA* fused to an SV40 NLS was PCR amplified from  $P_{PHYA}$ :PHYA-NLS-GFP5 (Genoud et al., 2008) using the primers ah010 and ah385. The PCR fragment was digested with XbaI-SpeI and ligated in sense orientation into D153ah-*phyA* Y242H to replace the wild-type fragment. The fragment coding for *phyA* Y242H-NLS was then transferred to pPPO30A as described for *phyA* Y242H.

pCHF80 is a T-DNA vector, which contains a  $P_{35S}$ :CFP-BamHI-AvrII-XbaI- $\text{Ter}_{RbcS}$  cassette and *bar* as selectable marker, and was obtained as follows. CFP (mCerulean) (Rizzo et al., 2004) was PCR amplified using the primers ah093 and ah094, digested with BglII-SpeI and ligated into the BamHI-XbaI site of pCHF5 (Hiltbrunner et al., 2005).

pCHF80-FHY1 is a T-DNA vector containing a  $P_{35S}$ :CFP-FHY1- $Ter_{RbcS}$  cassette. It was obtained by cutting FHY1 from pBS II KS-FHY1 (Hiltbrunner et al., 2005) using BamHI and SpeI and ligating the FHY1 fragment into pCHF80 cut with BamHI and XbaI.

pGADT7ah-PIF1  $\Delta$ bHLH is a yeast two hybrid vector containing PIF1 1-275 fused to the GAL4 AD. PIF1 1-275 was PCR amplified from total cDNA using the primers ah212 and wn4. The PCR fragment was cut with XbaI-SpeI and ligated in sense orientation into the XbaI-SpeI site of pGADT7-FHY1 (Hiltbrunner et al., 2005) to replace FHY1.

pCGADT7ah is a yeast two hybrid AD vector containing the multiple cloning site at the 5' end of the GAL4 AD (i.e., the GAL4 AD is fused to the C terminus of the protein to be expressed) and was obtained as follows. MCS-GAL4 AD was PCR amplified from pGADT7 using the primers ah521 and ah522, cut with HindIII and ligated in sense orientation into pGADT7 digested with HindIII to replace the fragment containing GAL4 AD-MCS.

pCGADT7ah-phyA is a yeast two hybrid vector containing phyA-GAL4 AD. It was generated by cutting phyA from pBS II KS-phyA (Hiltbrunner et al., 2005) with BamHI-SpeI and ligating it into the BamHI-XbaI site of pCGADT7ah.

pGAD424-PIF3, pGADT7-FHY1 and pGADT7-FHL are yeast two hybrid vectors containing GAL4 AD-PIF3, -FHY1 and -FHL, respectively. D153ah-phyA is a yeast two hybrid vector, which contains phyA-GAL4 BD. pCHF70-FHY1 is a T-DNA vector containing a  $P_{35S}$ :YFP-FHY1- $Ter_{RbcS}$  cassette. All these constructs have been described previously (Hiltbrunner et al., 2006; Hiltbrunner et al., 2005; Ni et al., 1998).

### Transgenic Lines

Transgenic lines used in this study were obtained by Agrobacterium mediated transformation using the floral dip method (Clough and Bent, 1998; Davis et al., 2009) or by crossing pre-existing lines. Selection for plants resistant to BASTA was done as described (Block et al., 1987). For selection of plants resistant to Butafenacil the commercially available herbicide Inspire (Syngenta Agro AG, Diersdorf, Switzerland) was used. Plants were grown on soil and sprayed with Inspire (7.6  $\mu$ l per liter tap water) 1 week after germination. Double transgenic lines expressing phyA Y242H-YFP/phyA-CFP (*phyA-201*  $P_{PHYA}$ :PHYA Y242H-YFP x *phyA-201*  $P_{PHYA}$ :PHYA-CFP) and phyA Y242H-YFP/CFP-FHY1 (*phyA-201*  $P_{PHYA}$ :PHYA Y242H-YFP x *fhv1-1*  $P_{35S}$ :CFP-FHY1) were obtained by crossing the respective single transgenic lines. To obtain *hy5-215* expressing phyA Y242H-NLS-YFP Col-0  $P_{PHYA}$ :PHYA Y242H-NLS-YFP plants were crossed into *hy5-215* background.

### Plant Growth

Seedlings used for protein extraction, microscopy or photographs were grown in petri dishes on 1/2x MS, 0.7% w/v agar. After sowing the plates were incubated for 2 days in the dark at 4°C followed by 4 hr in white light to induce germination. The plates were then grown at 23°C in D, FR (15  $\mu$ mol/(m<sup>2</sup>s), 730 nm, 128 nm FWHM) or R (12  $\mu$ mol/(m<sup>2</sup>s)), 670 nm, 20 nm FWHM) for the time indicated in the figure legends.

### Quantitative PCR

For qPCR seedlings were grown at 25°C in petri dishes on four layers of wet filter paper. The seeds were imbibed for 2 d at 6°C in the dark. Germination was induced by 24 hr irradiation with white light. For the analysis in Figure 3C the seedlings were grown in D for 5 days, exposed to R (650 nm; 0.042  $\mu$ mol/(m<sup>2</sup>s)) for 30 s and incubated in D for different time periods before harvesting. The seedlings used for the experiment in Figure 3D were grown in D for 4 days, either kept in D for another 24 hr or incubated in R (34.2  $\mu$ mol/(m<sup>2</sup>s), 656 nm, 24 nm FWHM), FR (45.3  $\mu$ mol/(m<sup>2</sup>s), 730 nm, 128 nm FWHM), B (10.6  $\mu$ mol/(m<sup>2</sup>s), 436 nm, 43 nm FWHM) or W (35.4  $\mu$ mol/(m<sup>2</sup>s), 340-850 nm) for 24 hr and harvested. Harvested seedlings were frozen in liquid nitrogen and stored at -80°C until RNA extraction. Total RNA from seedlings was isolated with Plant RNA reagent (Invitrogen, Darmstadt, Germany) according to the manufacturers protocol. Purification and on-column DNaseI digestion was performed by using the RNeasy mini Kit from QIAGEN (Hilden, Germany). After first-strand cDNA synthesis, the RT-PCR was accomplished by using an ABI Prism7300 (Applied Biosystems, Carlsbad CA, USA). FAM- and JOE-reporter dyes (5' end) were used for the TaqMan probes. The standard curve method (Livak, 1997) was used for the calculation of relative transcript quantities. Data were first normalized to the corresponding ACTIN1 mRNA levels and then calculated relative to a specific sample. Data represent averages of two biological replicates. Sequences of primers and probes used for Real-Time RT-PCR: ACTIN1 forward primer: 5'-GGC TCC AAG CAG CAT GAA G-3', ACTIN1 reverse primer: 5'-ACC CTC CAA TCC AGA CAG AGT ATT-3', ACTIN1 probe: JOE-5'-CAA AGT CGT TGC CCC TCC AGA GAG G-3'-BHQ1; PRR9 forward primer: 5'-CCG AAT CAC ATG AAA AGT TAA GAA AA-3', PRR9 reverse primer: 5'-CGG AAG CTT ACG CTT GAT GAT C-3', PRR9 probe: FAM-5'-AGC GCC ACA ACG AGC AGC AAC C-3'-TAMRA; CAB2 forward primer: 5'-GAG AGG CCG AGG ACT TGC TT-3', CAB2 reverse primer: 5'-CTC TGG GTC GGT AGC CAA AC-3', CAB2 probe: FAM-5'-ACC CCG GTG GCA GTT TCG ACC-3'-TAMRA.

### Characterization of the phyA C323A Mutant

Transgenic *Arabidopsis* seedlings expressing phyA C323A-YFP are fully etiolated when grown in FR (Figure S2A), phyA C323A does not interact with FHY1 under any light treatment (Figures 2A and S2B) and phyA C323A-YFP is not transported into nucleus in seedlings exposed to FR (Figure S2C). Moreover, phyA C323A-YFP is not degraded in R (Figure S2C) and does not form sequestered areas of phytochrome (SAPs), which are Pfr dependent cytosolic complexes consisting of ubiquitin and phyA and which have been implicated in the degradation of phyA (Jabben et al., 1989; Speth et al., 1987; Figure S2D). In contrast, wild-type phyA promotes

hypocotyl growth inhibition in FR, interacts with FHY1 when activated by light, rapidly accumulates in the nucleus in response to FR, forms SAPs and is degraded in R (Figures 2A and S2). Thus, hypocotyl growth inhibition, interaction with FHY1, transport into the nucleus, formation of SAPs and degradation depend on Pfr, supporting the notion that phyA C323A cannot be converted to Pfr. The idea that phytochromes, which are unable to bind the chromophore, are different from Pfr is also supported by several phyB mutants affected in chromophore binding (Kikis et al., 2009).

Plant phytochromes are obligate dimers (Rockwell et al., 2006) but dimerization does not depend on Pfr. This is consistent with our yeast two hybrid data (Figure S2B) as well as with data by Clack et al. (2009), showing that phyA forms dimers in Pr. Importantly, in our yeast two hybrid analyses also phyA C323A dimerized with phyA (Figure S2B). In summary, phyA C323A behaves like wild-type phyA in Pr, confirming that phyA C323A is different from Pfr and suggesting that it is either in Pr or in a state, which is more similar to Pr than to Pfr.

### Analytical Description of PhyA Kinetics

The reaction scheme of Figure 4 (main text) can be rewritten in terms of the major components involved into the phytochrome A interaction network, see Figure 4. It is cast in a system of coupled ordinary differential equations describing the time evolution of the network.

$$\begin{aligned}
 \dot{P}_R^c &= k_s + k_2 P_{FR}^c + \beta C_R^c - (k_1 + k_{dr} + k_{inA} + \gamma F^c) P_R^c \\
 \dot{P}_{FR}^c &= k_1 P_R^c + \alpha C_{FR}^c - (k_2 + k_d + k_{inA} + k_c F^c) P_{FR}^c \\
 \dot{C}_R^c &= k_2 C_{FR}^c + \gamma P_R^c F^c - (k_1 + \beta + k_{inC}) C_R^c \\
 \dot{C}_{FR}^c &= k_1 C_R^c + k_c P_{FR}^c F^c - (k_2 + \alpha + k_{inC}) C_{FR}^c \\
 \dot{F}^c &= \beta C_R^c + \alpha C_{FR}^c + k_{exF} F^n - (k_{inF} + k_c P_{FR}^c + \gamma P_R^c) F^c \\
 \dot{P}_R^n &= k_2 P_{FR}^n + \beta C_R^n + k_{inA} P_R^n - (k_1 + k_{dr} + \gamma F^n) P_R^n \\
 \dot{P}_{FR}^n &= k_1 P_R^n + \alpha C_{FR}^n + k_{inA} P_{FR}^n - (k_2 + k_d + k_c F^n) P_{FR}^n \\
 \dot{C}_R^n &= k_{inC} C_R^c + \gamma P_R^n F^n + k_2 C_{FR}^n - (k_1 + \beta) C_R^n \\
 \dot{C}_{FR}^n &= k_c P_{FR}^n F^n + k_{inC} C_{FR}^c + k_1 C_R^n - (k_2 + \alpha) C_{FR}^n \\
 \dot{F}^n &= k_{inF} F^c + \alpha C_{FR}^n + \beta C_R^n - (k_{exF} + k_c P_{FR}^n + \gamma P_R^n) F^n.
 \end{aligned} \tag{S1}$$

Parameters:  $k_s$  - phyA synthesis,  $k_1$  - photoconversion from Pr to Pfr,  $k_2$  - photoconversion from Pfr to Pr,  $k_{dr}$  - degradation of Pr,  $k_d$  - degradation of Pfr,  $k_{inA}$  - nuclear import of phyA-NLS,  $\alpha$  - FHY1/FHL-Pfr dissociation,  $\beta$  - FHY1/FHL-Pr dissociation,  $\gamma$  - FHY1/FHL-Pr association,  $k_c$  - FHY1/FHL-Pfr association,  $k_{inC}$  - FHY1/FHL-phyA complex nuclear import,  $k_{inF}$  - FHY1/FHL nuclear import,  $k_{exF}$  - FHY1/FHL nuclear export. As most of the biochemical parameters are unknown, a rescaling of concentration and time is applied, such that the total number of model parameters is reduced. We rescale the concentrations of the system with  $k_s/k_{dr}$ , such that the phytochrome level is normalized to unity in darkness. Time is expressed in units of half-life of  $P_R^c$ , i.e.,  $\tau = k_{dr} t$ . Furthermore, we assume mass conservation of FHY1/FHL, i.e., the initial FHY1/FHL concentration  $F_0$  is given by

$$F_0 = F^c + F^n + C_R^c + C_{FR}^c + C_R^n + C_{FR}^n \equiv const. \tag{S2}$$

Therefore, we express  $C_{FR}^c$  in terms of  $C_{FR}^c = F_0 - F^c - F^n - C_R^c - C_R^n - C_{FR}^n$ . The emerging dimensionless and reduced model system is described by the following system of ordinary differential equations:

$$\begin{aligned}
 \dot{p}_R^c &= 1 + \tilde{k}_2 p_{FR}^c + b_7 c_R^c - (\tilde{k}_1 + 1 + b_2 + b_8 f^c) p_R^c \\
 \dot{p}_{FR}^c &= \tilde{k}_1 p_R^c + b_4 (f_0 - f^c - f^n - c_R^c - c_R^n - c_{FR}^n) - (\tilde{k}_2 + b_1 + b_2 + b_3 f^c) p_{FR}^c \\
 \dot{c}_R^c &= \tilde{k}_2 (f_0 - f^c - f^n - c_R^c - c_R^n - c_{FR}^n) + b_8 p_R^c f^c - (\tilde{k}_1 + b_7 + b_9) c_R^c \\
 \dot{f}^c &= b_7 c_R^c + b_4 (f_0 - f^c - f^n - c_R^c - c_R^n - c_{FR}^n) + b_5 f^n - (b_6 + b_3 p_{FR}^c + b_8 p_R^c) f^c \\
 \dot{p}_R^n &= \tilde{k}_2 p_{FR}^n + b_7 c_R^n + b_2 p_R^n - (\tilde{k}_1 + 1 + b_8 f^n) p_R^n \\
 \dot{p}_{FR}^n &= \tilde{k}_1 p_R^n + b_4 c_{FR}^n + b_2 p_{FR}^c - (\tilde{k}_2 + b_1 + b_3 f^n) p_{FR}^n \\
 \dot{c}_R^n &= b_9 c_R^c + b_8 p_R^n f^n + \tilde{k}_2 c_{FR}^n - (\tilde{k}_1 + b_7) c_R^n \\
 \dot{c}_{FR}^n &= b_3 p_{FR}^n f^n + b_9 (f_0 - f^c - f^n - c_R^c - c_R^n - c_{FR}^n) + \tilde{k}_1 c_R^n - (\tilde{k}_2 + b_4) c_{FR}^n \\
 \dot{f}^n &= b_6 f^c + b_4 c_{FR}^n + b_7 c_R^n - (b_5 + b_3 p_{FR}^n + b_8 p_R^n) f^n.
 \end{aligned} \tag{S3}$$

Note that  $\dot{p}$  represents the time derivative with respect to  $\tau$ . Table S1 lists the dimensionless parameters together with their corresponding functional relation to the dimensional parameters.

For the qualitative parameter scan, we used Latin Hypercube Sampling (McKay et al., 1979), which uses a stratified sampling scheme to provide a better probabilistic coverage of the input space than a simple random sampling (Iman, 1999). For each parameter set the differential equations were integrated until  $\tau = 5$ , which roughly corresponds to 5 days ( $k_{dr}^{-1} \approx 24$  hr, Hennig et al., 2000). Subsequently it was checked whether the input conditions defined in Figure 4B of the main text were fulfilled, otherwise the parameter set was rejected.

### Sensitivity Analysis

We start by defining a sensitivity vector for a given function  $f$  depending on:  $s_i(\vec{p}) := |\partial f(\vec{p}) / \partial p_i|$  ( $|\cdot|$  represents the absolute value), which gives us the local dependence of the function  $f$  at parameter point  $\vec{p}$  on the parameter  $p_i$  irrespective of the sign of the derivative. We locally average the sensitivity by integrating over the individual directions:

$$S_i(\vec{p}) := \frac{1}{2\ell} \int_{p_i-\ell}^{p_i+\ell} s_i(\vec{p}) dp_i \quad (S4)$$

where  $\ell$  denotes the range of integration. We integrate each parameter over one order of magnitude, i.e.,  $\ln(p_i) \in [-0.5 + \ln(p_i), \ln(p_i) + 0.5]$ , and approximate the integral by the corresponding discrete sum using at least 10 equally spaced terms.

For every admissible parameter combination  $\vec{p}_n$  we obtain the sensitivity  $S_i(\vec{p}_n)$  of each parameter with respect to the peak position and the peak height. Further, we compute the averaged sensitivity for  $S_i$  each parameter by

$$\langle S_i \rangle := \frac{1}{N} \sum_{n=1}^N S_i(\vec{p}_n) \quad (S5)$$

where  $N$  is the number of admissible parameters found. Figure 5 of the main text shows the averaged sensitivity values  $\langle S_i \rangle$  for all kinetic constants of the phyA network depicted in Figure 4. To obtain the compartment-specificity of the sensitivities we varied  $b_1$  and  $b_4$ , resp., separately in the cytosol and the nucleus. Figure S5 shows representative trajectories of the impact of parameter variation on the peak position (A, B) or the peak height (C, D). Decreasing the Pfr degradation rate  $b_1$  shifted the maximal action almost always to shorter wavelength (Figure S5A). The observed nuclear-specific sensitivity of the peak position to  $b_1$  variation can be understood as follows. A peak in the far-red requires a flux over a  $k_2$  (type II) edge as well as a flux over a  $k_1$  (type I) edge. The type II edge is located in the nucleus while two type I edges, one in the cytosol and one in the nucleus, exist in the path from synthesis to the effector. For many parameter combinations the type I edge in the nucleus contributes stronger to the peak producing behavior of the network and hence the sensitivity of  $b_1$  is larger in the nucleus than in the cytosol. Further, although the Pfr-FHY1 complex dissociation rate  $b_4$  has a large average sensitivity as defined in Eq. (S5), the response of the network to a change in  $b_4$  is not uniform throughout the admissible parameter space (Figure S5B). The specific response of the network to a variation in  $b_4$  depends sensitively on the other parameters, i.e., on the region of the admissible parameter space. We can roughly distinguish two cases: (i) the Pfr-FHY1 complex formation rate  $b_3$  is sufficiently large. The particle flux in the network from synthesis to the  $p_{FR}^n$  pool is dominantly via  $p_R^c \rightarrow p_{FR}^c \rightarrow c_{FR}^c \rightarrow c_{FR}^n$ . Increasing  $b_4$  results in a weak shift of the peak to shorter wavelength and finally in a complete loss of the peak (Figure S5B, dashed black lines). (ii)  $b_3$  is relatively small. The particle flux in the network from synthesis to the  $p_{FR}^n$  pool is partly also via  $p_R^c \rightarrow c_R^c \rightarrow c_{FR}^c \rightarrow c_{FR}^n$ . Increasing  $b_4$  results in a shift of the peak to longer wavelength and again finally in a complete loss of the peak (Figure S5B, solid black lines). The intricate behavior of the network results from the non-linear coupling between the nuclear and the cytosolic loops via the FHY1/FHL cycling. Note that in all cases considered in the sensitivity analysis  $b_4$  is smaller than the photo-conversion rate  $\max_{\lambda \in [640, 720]} \tilde{k}_2(\lambda)$ . The narrow distribution found in the parameter sampling procedure (Figure S5E) is largely due to the input condition (Figure 4 of the main text) that the action spectrum exhibits a peak somewhere in the range  $\lambda \in [640\text{nm}, 720\text{nm}]$ .

We considered the impact of parameter variation of the Pfr degradation rate  $b_1$  (C) and the FHY1/FHL initial condition  $f_0$  (D) on the peak height and found that for increasing  $b_1$  the relative height of the action spectrum peak decreased, whereas for smaller  $b_1$  we found an increased peak height. The opposite held for the variation of the FHY1/FHL initial condition (D). Increasing  $f_0$  resulted in an increased height of the action spectrum peak.

The  $f_0$  and the  $b_9$  distributions (Figure S5E) are mainly restrained by the requirement that upon light treatment more than 10% of the phyA accumulates in the nucleus. Moreover, large values in the distribution for  $b_7$  are suppressed mostly by the input condition that not more than 5% of phyA is in the nucleus in darkness.

### Additional Simulation Results

#### FHY1-phyA Binding and Amount of Complexes in Different Light Conditions

We investigated the dependence of the FHY1 binding strength to Pfr and Pr on the presence of the relative amount of complexes in different light conditions. For each admissible parameter combination and the corresponding  $b_3/b_8$  ratio, we studied the presence of

FHY1-phyA complexes, irrespective of cytosolic or nuclear localization and Pr or Pfr bound, relative to the total amount of phyA in red light,  $\lambda = 660$  nm, or far red light,  $\lambda = 726$  nm. Figure 7C shows that there is no correlation between the FHY1 binding strength to Pfr or Pr and the abundance of FHY1-phyA complexes in far-red or red light. Moreover it can be deduced by Figure 7C that for most of the admissible parameter combinations (79%, boxed) the relative amount of complexes is higher in far-red light than in red light.

### Pfr Amount over Time

For almost all admissible parameter combinations a nuclear HIR, i.e., the amount of unbound nuclear Pfr is highest in far-red light, has been observed, see Figure 5A of main text. We studied the abundance of Pfr over time, Figure 7D and 7E. If cytosolic and nuclear Pfr is recorded, Figure 7D, red light (660 nm, black line) yields the highest amount of relative Pfr after 5 days of irradiation. If, however, nuclear Pfr, i.e., free and complex-bound, is recorded, it can be observed that its amount after 5 days is maximal for 712 nm, see Figure 7E. Therefore it is likely that nuclear Pfr rather than the total amount of Pfr in a cell triggers the physiological response.

### Analysis of the Shifting Module

The light induced conformational transitions from the red light absorbing, Pr, and far-red light absorbing, Pfr, form can be described by the first order reaction rates  $k_1 = \sigma_1(\lambda)N$  and  $k_2 = \sigma_2(\lambda)N$ , where  $N$  denotes the fluence rate and  $\sigma_{1/2}(\lambda)$  denote the wavelength specific photoconversion cross-sections. These cross-sections have been measured and it is common to use the averaged values given in Mancinelli (1994). It is common in photobiology to use the unit  $\mu\text{mol}/(\text{m}^2\text{s})$  for the photon flux. To come to the standard measure used for intensity  $I$  in physics, given in  $\text{Watt}/\text{m}^2$ , one has to multiply the flux  $f$  given in  $\text{mol}/(\text{m}^2\text{s})$  by the energy of a photon of the particular wavelength  $\lambda$  which reads:  $E_\lambda = hc/\lambda$  ( $h$  is the Planck constant,  $c$  the velocity of light), and further multiply it by Avogadro constant  $N_A$ . It follows for the intensity  $I$  of the irradiance:  $I = fE_\lambda N_A$ . If one uses  $[N] = \mu\text{mol}/(\text{m}^2\text{s})$ , the cross-sections have the unit  $[\sigma_{1/2}(\lambda)] = \text{m}^2/\text{mol}$ . For the following analysis it is convenient to use dimensionless parameters. To this end we rewrite the transition rates:  $k_1 = \tilde{N}\tilde{\sigma}_1(\lambda)$ ,  $k_2 = \tilde{N}\tilde{\sigma}_2(\lambda)$ . The rescaled fluence rate  $\tilde{N}$  has now the unit  $\text{s}^{-1}$  and is given by:  $\tilde{N} = N/\sigma_t$ , where  $\sigma_t = \sqrt{(\sigma_1^m)^2 + (\sigma_2^m)^2}$  ( $\sigma_1^m$ ,  $\sigma_2^m$  are the maxima of corresponding cross-section). The cross-sections are accordingly rescaled:  $\tilde{\sigma}_1 = \cos(\phi)\sigma_1/\sigma_t$  and  $\tilde{\sigma}_2 = \sin(\phi)\sigma_2/\sigma_t$ , where the angle  $\phi$  is defined via  $\tan(\phi) = \sigma_2^m/\sigma_1^m$ . It follows that  $[\tilde{\sigma}_{1/2}] = 1$ . The values are roughly:  $\sigma_t \approx 5580 \text{ m}^2/\text{mol}$ , and  $\tilde{N} \approx 0.33 \text{ min}^{-1}$  for  $N = 1 \mu \text{ mol}/(\text{m}^2\text{s})$ .

### Single wavelength shifting network

We start by considering the small linear three node network given in Figure 7C of the main text. The direction from the influx node X to the effector node Z (dashed circle) defines the forward direction. Further, we always attach an edge of type I (see main text) to the node with the influx (X). The steady state result for the effector state Z reads:

$$\tilde{z} = \frac{\tilde{\sigma}_1 \tilde{\sigma}_2}{\beta \tilde{\sigma}_1^2 + \alpha \gamma (2\tilde{\sigma}_2 + \beta \gamma) + \tilde{\sigma}_1 (\tilde{\sigma}_2 + \beta \gamma) (1 + \alpha)} = : \Gamma \quad (\text{S6})$$

where  $\alpha = \lambda_x/\lambda_z$ ,  $\beta = \lambda_y/\lambda_z$ ,  $\gamma = \lambda_z/\tilde{N}$ , and  $\tilde{z} = z\lambda_z/\omega$  ( $\omega$  is the influx into node X,  $\lambda_x$  degradation rate of state X, etc.). The quantity  $\omega/\lambda_z$  used to rescale  $z$  is maximum of the state  $z$  if the attenuation of the network is zero, i.e., the influx  $\omega$  is without loss transmitted via the intermediate node Y to the effector Z. It follows that  $\tilde{z} \in [0, 1]$ . Eq. S6 also defines the transmission function  $\Gamma$  if one concatenates the networks without feedback as we will discuss in the next section. If the wavelength dependence of the effector Z is dominated by the wavelength characteristics of the red light absorbing form Pr, i.e., by  $\tilde{\sigma}_1$ , the response peak will be in red light, if the wavelength dependence of Z is dominated by the wavelength characteristics of the far-red light absorbing form Pfr, i.e., by  $\tilde{\sigma}_2$ , the action or response peak will be in far-red light. In the latter case the network will produce the required wavelength shift. We discuss some limiting cases:

i) low fluence rate,  $\gamma \rightarrow \infty$ :

$$\tilde{z} = \frac{\tilde{\sigma}_1 \tilde{\sigma}_2}{\alpha \beta \gamma^2} + \mathcal{O}(\gamma^{-4}) \quad (\text{S7})$$

ii) high fluence rate,  $\gamma \rightarrow 0$ :

$$\tilde{z} = \frac{\tilde{\sigma}_2}{\beta \tilde{\sigma}_1 + \tilde{\sigma}_2 (1 + \alpha)} + \mathcal{O}(\gamma) \quad (\text{S8})$$

iii) stable initial state X,  $\alpha \rightarrow 0$ :

$$\tilde{z} = \frac{\tilde{\sigma}_2}{\beta \tilde{\sigma}_1 + \tilde{\sigma}_2 + \beta \gamma} + \mathcal{O}(\alpha) \quad (\text{S9})$$

iv) stable intermediate state Y,  $\beta \rightarrow 0$ :

$$\tilde{z} = \frac{\tilde{\sigma}_1}{(1 + \alpha)\tilde{\sigma}_1 + \alpha\gamma} + \mathcal{O}(\beta) \quad (\text{S10})$$

To summarize these results: if the intermediate state Y is stable, i.e.,  $\beta \ll 1$  or  $\lambda_y \ll \lambda_z$ , the network cannot produce the wavelength shift, regardless of the fluence rate. In contrast, if the initial state is stable, i.e.,  $\alpha \ll 1$  or  $\lambda_x \ll \lambda_z$ , the action peak will be in far-red light and will be most pronounced for high fluence rates. Further, the high or low fluence rate limit is achieved if the ratio  $\gamma$  between the degradation rate of the effector Z and the fluence rate is large or small, respectively.

The behavior of  $\tilde{z}$  as a function of the wavelength  $\lambda$  can be visualized as follows: the function  $\tilde{z}$  describes a surface in  $\mathbb{R}^3$ :  $\mathbb{R}^2 \rightarrow \mathbb{R}^3$ ,  $(\tilde{\sigma}_1, \tilde{\sigma}_2) \mapsto (\tilde{\sigma}_1, \tilde{\sigma}_2, \tilde{z}(\tilde{\sigma}_1, \tilde{\sigma}_2))$ . The mapping  $\lambda \mapsto (\tilde{\sigma}_1(\lambda), \tilde{\sigma}_2(\lambda), \tilde{z}(\tilde{\sigma}_1(\lambda), \tilde{\sigma}_2(\lambda)))$  describes a path on this surface parametrized by the wavelength  $\lambda$ . If for the position  $\lambda_m$  of the maximum along this path  $\lambda_m > \lambda_{ib}$  holds ( $\lambda_{ib} \approx 702$  nm is the isobestic point, at which  $\tilde{\sigma}_1(\lambda_{ib}) = \tilde{\sigma}_2(\lambda_{ib})$ ), the network performs the desired wavelength shift from red to far-red. This can be seen in Figure S7. The path parametrized by  $\lambda$  is shown in red, the dashed line denotes  $\tilde{\sigma}_1 = \tilde{\sigma}_2$ , and the solid blue line denotes the location of the maximum in  $\tilde{\sigma}_1$ -direction. There is no true maximum in  $\tilde{\sigma}_2$ -direction. Starting at  $\lambda = 600$  nm,  $\tilde{\sigma}_1$  increases until its maximum, then the red curve turns back and  $\tilde{\sigma}_2$  increases. For low fluence rates ( $\gamma = 1.4$ ) in Figure S7A the maximum of  $\tilde{z}$  along the path (black circle) is in the  $\tilde{\sigma}_1 > \tilde{\sigma}_2$  region, i.e., for  $\lambda < \lambda_{ib}$ . In contrast, for high fluence rates ( $\gamma = 0.1$ ) in Figure 7SB the maximum is in the  $\tilde{\sigma}_1 < \tilde{\sigma}_2$  region, i.e., for  $\lambda > \lambda_{ib}$ .

#### Sharpening the action spectrum by concatenating shifting modules

We consider the serial connection of networks discussed in the previous section, where we neglect for the sake of simplicity feedbacks between the modules; as long as the feedback is weak the results derived in the following will still hold. The outcome of the  $n$ -th module is given by:

$$z_n = \frac{k_c}{\lambda_z} \Gamma z_{n-1} \quad (\text{S11})$$

where  $\Gamma$  is the transmission function given by Eq. S6,  $\lambda_z$  is the degradation rate of the effector state Z and  $k_c$  is the coupling rate. Setting  $z_0 = \omega$  we find:

$$z_n = \frac{\omega}{\lambda_z} \left( \frac{k_c}{\lambda_z} \right)^{n-1} \Gamma^n. \quad (\text{S12})$$

In order to compare the effect of varying  $n$ , the length of the network chain, we normalize  $z_n$  with  $C_n$  given by:

$$C_n = \int_0^{\infty} \frac{\omega}{\lambda_z} \left( \frac{k_c}{\lambda_z} \right)^{n-1} \Gamma^n(\lambda) d\lambda. \quad (\text{S13})$$

It follows:

$$\tilde{z}_n = \frac{z_n}{C_n} = \frac{\Gamma^n}{\int_0^{\infty} \Gamma^n(\lambda) d\lambda}. \quad (\text{S14})$$

The resulting action spectra or curves  $\tilde{z}_n(\lambda)$  for  $n = 1, 2, 3$  are shown in Figure 7D. We estimated the number  $n$  of shifting modules in action in planta by fitting Eq. (S14) to the measured action spectrum in Dieterle et al. (2001). Because the parameters are not identifiable, we determine those parameter sets for which we obtain a reasonable good fit (coefficient of determination  $R^2 \geq 0.96$ ). For  $n$  we obtained a distribution with mean  $n = 3.9 \pm 0.4$ . A fit with  $n = 4$  is shown in Figure S1 (dashed line).

#### SUPPLEMENTAL REFERENCES

Block, M.D., Botterman, J., Vandewiele, M., Dockx, J., Thoen, C., Gosselé, V., Movva, N.R., Thompson, C., Montagu, M.V., and Leemans, J. (1987). Engineering herbicide resistance in plants by expression of a detoxifying enzyme. *EMBO J.* 6, 2513–2518.

Clack, T., Shokry, A., Moffet, M., Liu, P., Faul, M., and Sharrock, R.A. (2009). Obligate heterodimerization of Arabidopsis phytochromes C and E and interaction with the PIF3 basic helix-loop-helix transcription factor. *Plant Cell* 21, 786–799.

Clough, S.J., and Bent, A.F. (1998). Floral dip: a simplified method for Agrobacterium-mediated transformation of Arabidopsis thaliana. *Plant J.* 16, 735–743.

Cole, N.B., Smith, C.L., Sciaky, N., Terasaki, M., Edidin, M., and Lippincott-Schwartz, J. (1996). Diffusional mobility of Golgi proteins in membranes of living cells. *Science* 273, 797–801.

- Davis, A.M., Hall, A., Millar, A.J., Darrah, C., and Davis, S.J. (2009). Protocol: Streamlined sub-protocols for floral-dip transformation and selection of transformants in *Arabidopsis thaliana*. *Plant Methods* 5, 3.
- Dieterle, M., Zhou, Y.C., Schäfer, E., Funk, M., and Kretsch, T. (2001). EID1, an F-box protein involved in phytochrome A-specific light signaling. *Genes Dev.* 15, 939–944.
- Genoud, T., Schweizer, F., Tscheuschler, A., Debrieux, D., Casal, J.J., Schäfer, E., Hiltbrunner, A., and Fankhauser, C. (2008). FHY1 mediates nuclear import of the light-activated phytochrome A photoreceptor. *PLoS Genet.* 4, e1000143.
- Hanin, M., Volrath, S., Bogucki, A., Briker, M., Ward, E., and Paszkowski, J. (2001). Gene targeting in *Arabidopsis*. *Plant J.* 28, 671–677.
- Hennig, L., Büche, C., and Schäfer, E. (2000). Degradation of phytochrome A and the high irradiance response in *Arabidopsis*: a kinetic analysis. *Plant Cell Environ.* 23, 727–734.
- Hiltbrunner, A., Tscheuschler, A., Viczián, A., Kunkel, T., Kircher, S., and Schäfer, E. (2006). FHY1 and FHL act together to mediate nuclear accumulation of the phytochrome A photoreceptor. *Plant Cell Physiol.* 47, 1023–1034.
- Hiltbrunner, A., Viczián, A., Bury, E., Tscheuschler, A., Kircher, S., Tóth, R., Honsberger, A., Nagy, F., Fankhauser, C., and Schäfer, E. (2005). Nuclear accumulation of the phytochrome A photoreceptor requires FHY1. *Curr. Biol.* 15, 2125–2130.
- Iman, R.L. (1999). Latin Hypercube Sampling. In *Encyclopedia of Statistical Sciences*. Update Volume 3. (New York: Wiley), 408–411.
- Jabben, M., Shanklin, J., and Vierstra, R.D. (1989). Ubiquitin-phytochrome conjugates. Pool dynamics during *in vivo* phytochrome degradation. *J. Biol. Chem.* 264, 4998–5005.
- Kikis, E.A., Oka, Y., Hudson, M.E., Nagatani, A., and Quail, P.H. (2009). Residues clustered in the light-sensing knot of phytochrome B are necessary for conformer-specific binding to signaling partner PIF3. *PLoS Genet.* 5, e1000352.
- Livak, K.J. (1997). User Bulletin No. 2: ABI PRISM 7700 Sequence Detection System (Foster City, CA: PE Applied Biosystems).
- Li, X., Volrath, S.L., Nicholl, D.B., Chilcott, C.E., Johnson, M.A., Ward, E.R., and Law, M.D. (2003). Development of protoporphyrinogen oxidase as an efficient selection marker for *Agrobacterium tumefaciens*-mediated transformation of maize. *Plant Physiol.* 133, 736–747.
- Mancinelli, A.L. (1994). The physiology of phytochrome action. In *Photomorphogenesis in Plants*, R.E. Kendrick and G.M.H. Kronenberg, eds. (Dordrecht: Kluwer Academic Publishers), pp. 211–269.
- McKay, M.D., Conover, W.J., and Beckman, R.J. (1979). A comparison of three methods for selecting values of input variables in the analysis of output from a computer code. *Technometrics* 21, 239–245.
- Ni, M., Tepperman, J.M., and Quail, P.H. (1998). PIF3, a phytochrome-interacting factor necessary for normal photoinduced signal transduction, is a novel basic helix-loop-helix protein. *Cell* 95, 657–667.
- Rizzo, M.A., Springer, G.H., Granada, B., and Piston, D.W. (2004). An improved cyan fluorescent protein variant useful for FRET. *Nat. Biotechnol.* 22, 445–449.
- Rockwell, N.C., Su, Y.S., and Lagarias, J.C. (2006). Phytochrome structure and signaling mechanisms. *Annu. Rev. Plant Biol.* 57, 837–858.
- Speth, V., Otto, V., and Schäfer, E. (1987). Intracellular localization of phytochrome and ubiquitin in red-light-irradiated oat coleoptiles by electron microscopy. *Planta* 171, 332–338.
- Tillemans, V., Leponce, I., Rausin, G., Dispa, L., and Motte, P. (2006). Insights into nuclear organization in plants as revealed by the dynamic distribution of *Arabidopsis* SR splicing factors. *Plant Cell* 18, 3218–3234.

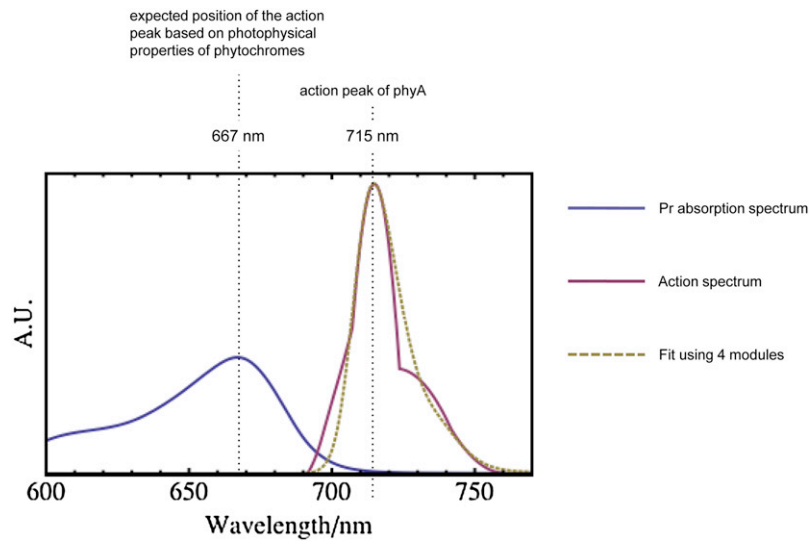


**Figure S1. Shift in Spectral Sensitivity, Related to Figure 4 and Figure 7**

Shift of the phyA action peak from R to FR. Pr absorption spectrum (blue line, redrawn from Mancinelli, 1994) and phyA action spectrum (red line, redrawn from Dieterle et al., 2001). The position of the phyA action peak as expected based on the photophysical properties of phytochromes and the actual phyA action peak are indicated (A.U., arbitrary units). The dashed line shows the fit using four concatenated shifting modules as shown in Figures 7C and 7D and specified in Equations (6) and (14), resp.

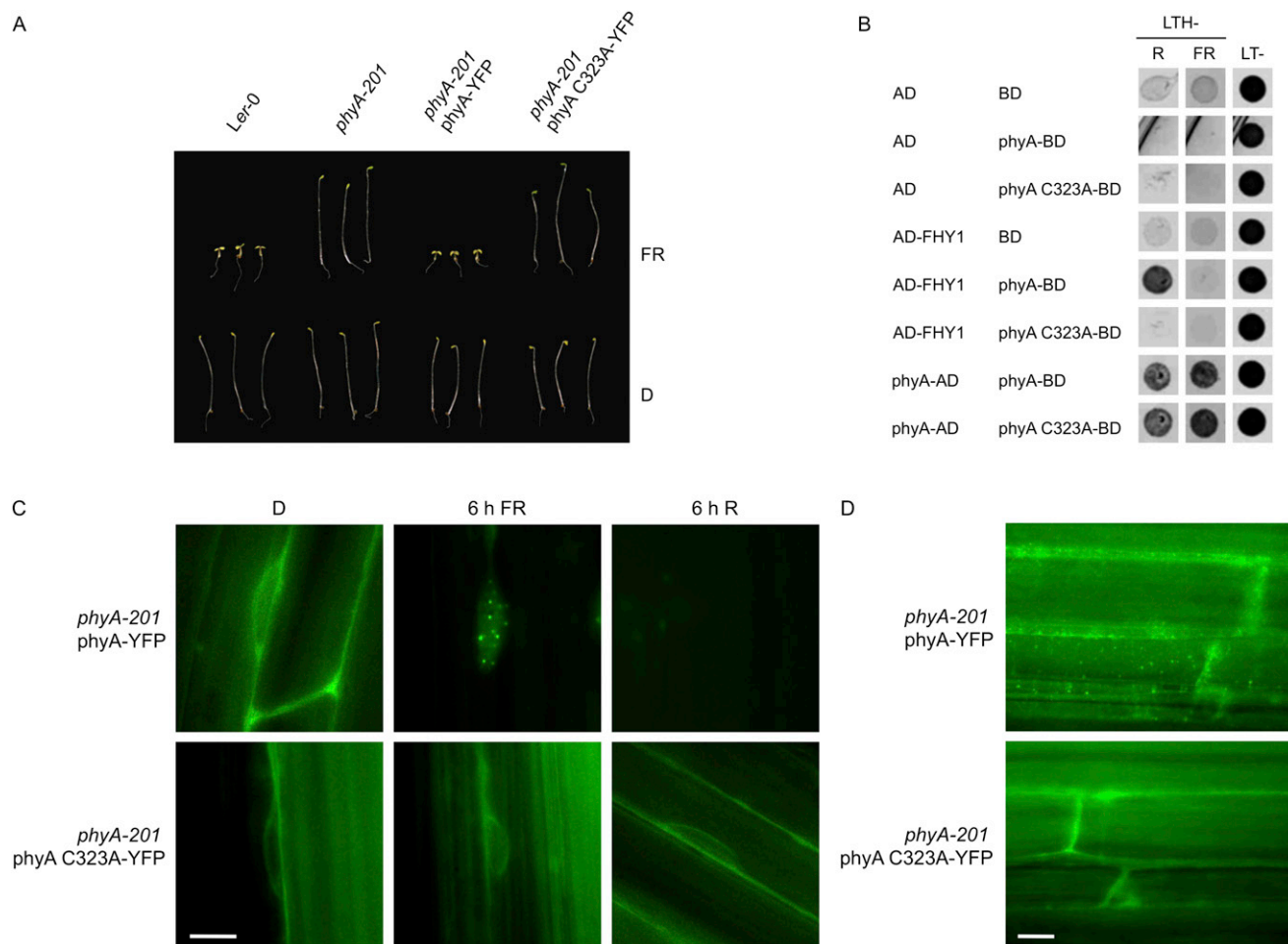


**Figure S2. Pfr Is Essential for PhyA Nuclear Transport, Related to Figure 2**

(A) The phyA C323A mutant is insensitive to FR. *Ler-0*, *phyA-201* as well as *phyA-201* seedlings expressing either  $P_{PHYA}$ :PHYA-YFP or  $P_{PHYA}$ :PHYA C323A-YFP were grown for 4 days in D or FR ( $15 \mu\text{mol}/(\text{m}^2\text{s})$ ).

(B) PhyA C323A is not affected in dimerization. Yeast cells co-expressing the indicated plasmid constructs were grown on non-selective plates (CSM LT-) or on selective plates (CSM LTH-) supplemented with 1 mM 3-AT and 10  $\mu\text{M}$  PCB. The selective plates were incubated in FR ( $15 \mu\text{mol}/(\text{m}^2\text{s})$ ) or R ( $1 \mu\text{mol}/(\text{m}^2\text{s})$ ).

(C and D) PhyA C323A-YFP does not accumulate in the nucleus. *phyA-201* seedlings expressing either  $P_{PHYA}$ :PHYA-YFP or  $P_{PHYA}$ :PHYA C323A-YFP were grown for 4 days in D. The seedlings were used either directly (D) for microscopic analysis or after a 6 hr FR ( $15 \mu\text{mol}/(\text{m}^2\text{s})$ ) or R ( $12 \mu\text{mol}/(\text{m}^2\text{s})$ ) treatment. The scale bar represents 5  $\mu\text{m}$ . (D) PhyA C323A-YFP does not form sequestered areas of phytochrome (SAPs).  $P_{PHYA}$ :PHYA-YFP or  $P_{PHYA}$ :PHYA C323A-YFP expressing *phyA-201* seedlings were grown for 4 days in D. The images were taken after 2 min irradiation with microscope light. The scale bar represents 10  $\mu\text{m}$ .



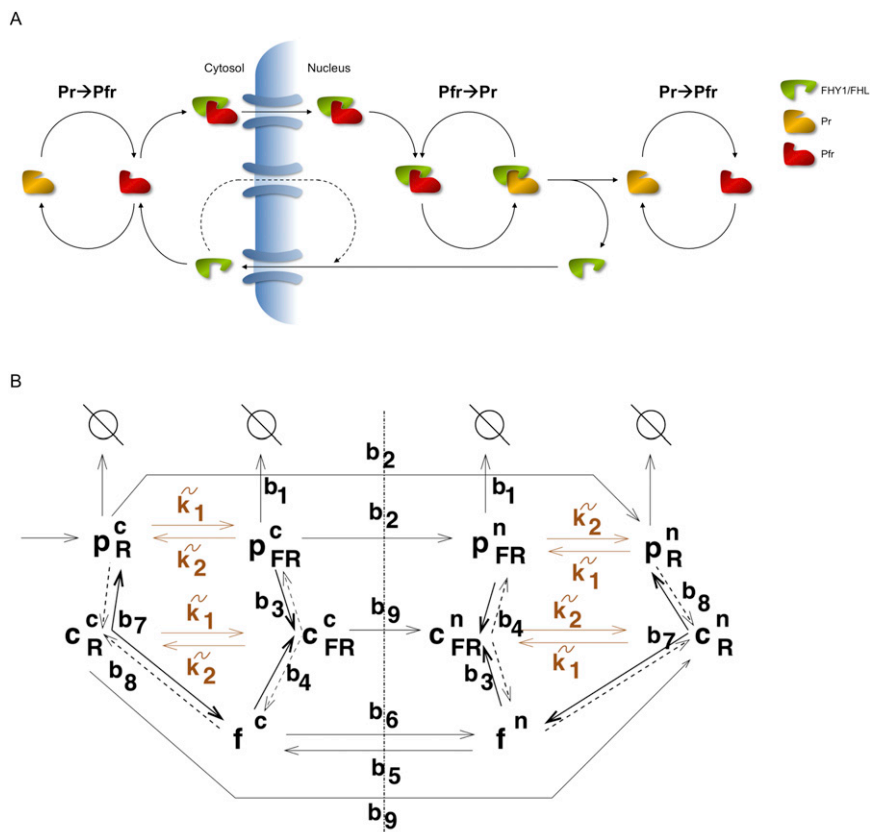


**Figure S4. PhyA Model, Related to Figure 4 and Table S2**

(A) Schematic representation of the model for phyA nuclear transport.

(B) Model for phyA action including all parameter names, which is cast into a system of ordinary differential equations given in Eqs. (S1) and (S3). Choosing appropriate kinetic values, it mimics different genotypes and light treatments, summarized in Table S2.  $p_R^c$ : cytosolic P<sub>r</sub>,  $p_{FR}^c$ : cytosolic P<sub>fr</sub>,  $f^c$ : cytosolic FHY1/FHL,  $c_R^c$ : cytosolic FHY1/FHL-P<sub>r</sub> complex,  $c_{FR}^c$ : cytosolic FHY1/FHL-P<sub>fr</sub> complex,  $p_R^n$ : nuclear P<sub>r</sub>,  $p_{FR}^n$ : nuclear P<sub>fr</sub>,  $f^n$ : nuclear FHY1/FHL,  $c_R^n$ : nuclear FHY1/FHL-P<sub>r</sub> complex,  $c_{FR}^n$ : nuclear FHY1/FHL-P<sub>fr</sub> complex.

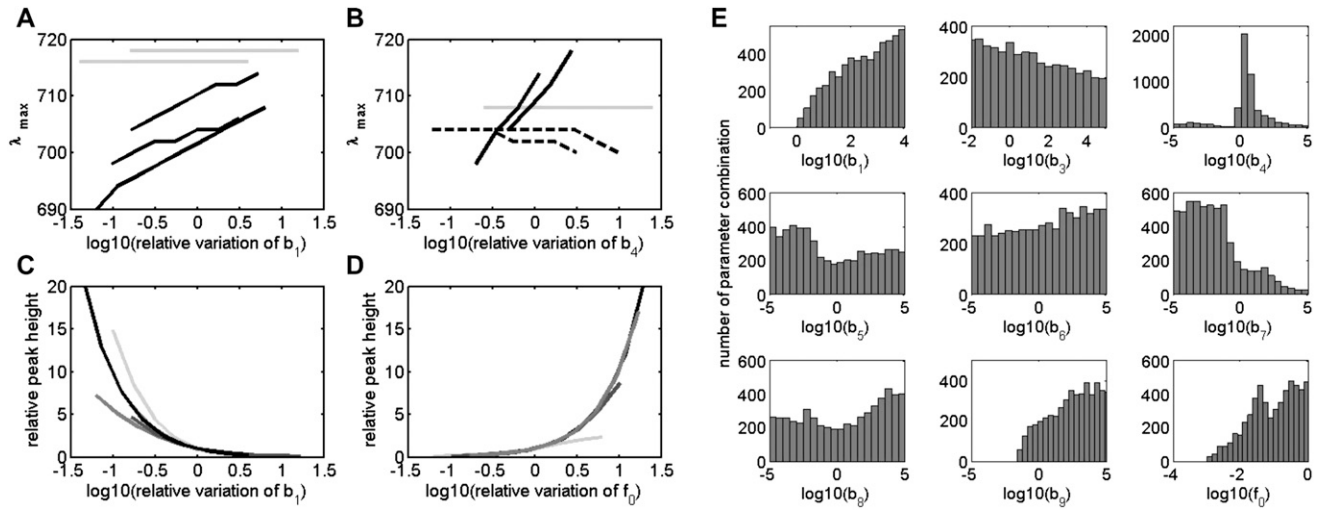


**Figure S5. Parameter Distributions and Effect of Parameter Variations, Related to Figure 5**

(A–D) Parameter variation and the corresponding peak position (A, B) or peak height (C, D). Representative trajectories are shown. Blunt ends denote exit of the admissible parameter space, i.e., the dynamic model fails at this parameter point to satisfy at least one of the conditions on the list given in Figure 4B. Note that although  $b_1$  and  $b_4$  are parameters with a large mean sensitivity as defined in Eq. (S5) for some parameter sets in the admissible space the network is insensitive to variations of  $b_1$  or  $b_4$ , resp., (A and B, gray solid lines). The response of the network to  $b_4$  variation (B) is not uniform throughout the admissible parameter space, but depends on the relative strength of  $b_3$  (dashed black lines: large  $b_3$ , solid black lines: small  $b_3$ ).

(E) Distribution of admissible parameters, i.e., of parameters reproducing the input conditions defined in Figure 4B and resulting in higher levels of phytochrome in the nucleus in FR than R ( $\text{phy}_{\text{nuc}}(660 \text{ nm}) < \text{phy}_{\text{nuc}}(720 \text{ nm})$ ;  $\text{phy}_{\text{nuc}} = p_{\text{R}}^{\text{n}} + p_{\text{FR}}^{\text{n}} + c_{\text{R}}^{\text{n}} + c_{\text{FR}}^{\text{n}}$ ).

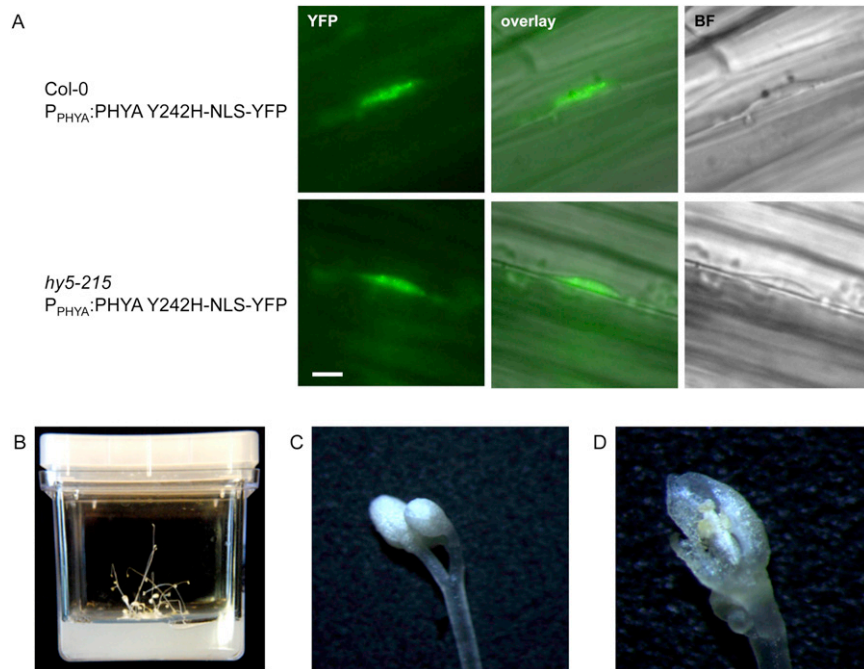


**Figure S6. PhyA Y242H-NLS-YFP Localizes to the Nucleus and Induces Flowering in Dark-Grown Plants, Related to Figure 6**

(A) Col-0 and *hy5-215* seedlings expressing P<sub>PHYA</sub>::PHYA Y242H-NLS-YFP were grown in D for 4 days and used for microscopy. The scale bar represents 5  $\mu$ m. BF, bright field.

(B–D) Col-0 plants expressing P<sub>PHYA</sub>::PHYA Y242H-NLS-YFP were grown for 6 weeks in the dark on 1/2x MS, 0.7% w/v agar supplemented with 1% w/v sucrose. In (D) a bud has been opened.

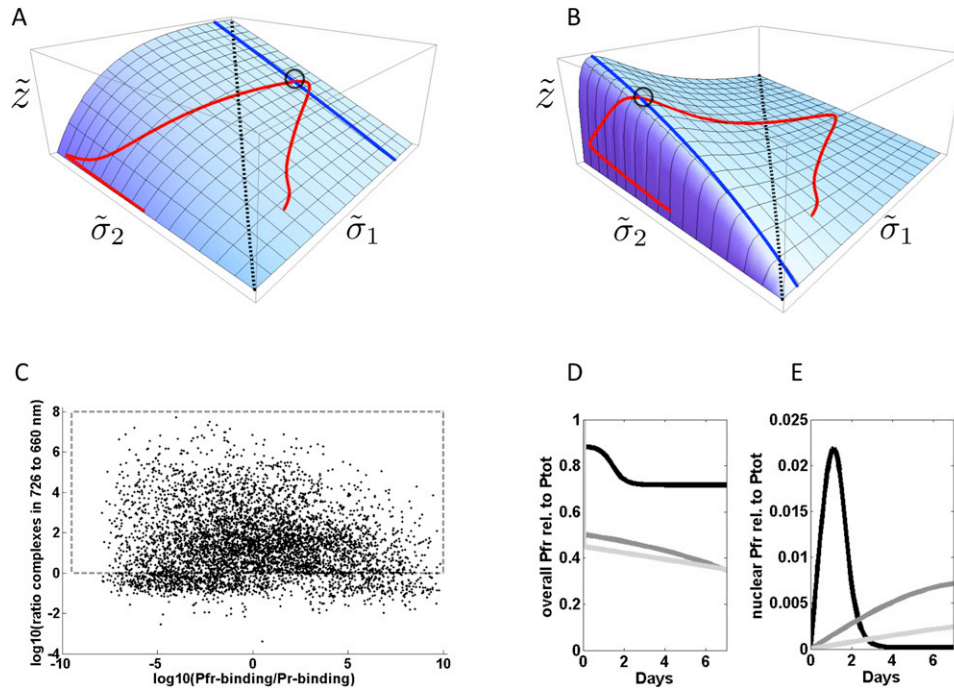


**Figure S7. Behavior of the Model, Related to Figure 5 and Figure 7**

(A and B) The different behavior of the shifting module defined in Figures 7C and Eq. (S6) for low fluence rates (A) and high fluence rates (B), resp. The height of the surface denotes the rescaled amount of the effector  $Z$ , while the red path denotes the variation of the rescaled absorption coefficients  $\tilde{\sigma}_1(\lambda)$  and  $\tilde{\sigma}_2(\lambda)$  as a function of the wavelength  $\lambda$ . The black circle points to the position of the maximum along the path on the surface. See section 'Analysis of the shifting module' for further explanation. Parameters used:  $\alpha = 0.3$ ,  $\beta = 1$ . (A)  $\gamma = 1.4$ , (B)  $\gamma = 0.1$ .

(C) Ratio of FHY1-phyA complexes in 726 to 660 nm in dependence on the ratio of the FHY1-Pfr/Pr binding rate. The box contains the admissible parameters for which the relative amount of FHY1-phyA complexes is larger at 726 nm than at 660 nm (79% of all admissible parameters).

(D and E) Pfr amount over time in different light conditions. The overall amount of Pfr (D) and nuclear Pfr (E) relative to Ptot over time was simulated in 660 nm (black), 712 nm (dark gray), and 726 nm (light gray).